

# First numerical observation of the Berezinskii-Kosterlitz-Thouless transition in language models

Yuma Toji,<sup>1</sup> Jun Takahashi,<sup>2</sup> Vwani Roychowdhury,<sup>3</sup> and Hideyuki Miyahara<sup>1,\*</sup>

<sup>1</sup> Graduate School of Information Science and Technology,  
Hokkaido University, Sapporo, Hokkaido 060-0814, Japan

<sup>2</sup> Institute for Solid State Physics, The University of Tokyo,  
5-1-5 Kashiwanoha, Kashiwa, Chiba 277-8581, Japan

<sup>3</sup> Henry Samueli School of Engineering and Applied Science,  
University of California, Los Angeles, California 90095

(Dated: December 3, 2024)

Several power-law critical properties involving different statistics in natural languages – reminiscent of scaling properties of physical systems at or near phase transitions – have been documented for decades. The recent rise of large language models (LLMs) has added further evidence and excitement by providing intriguing similarities with notions in physics such as scaling laws and emergent abilities. However, specific instances of classes of generative language models that exhibit phase transitions, as understood by the statistical physics community, are lacking. In this work, inspired by the one-dimensional Potts model in statistical physics we construct a simple probabilistic language model that falls under the class of context sensitive grammars (CSG), and numerically demonstrate an unambiguous phase transition in the framework of a natural language model. We explicitly show that a precisely defined order parameter – that captures symbol frequency biases in the sentences generated by the language model – changes from strictly 0 to a strictly nonzero value (in the infinite-length limit of sentences), implying a mathematical singularity arising when tuning the parameter of the stochastic language model we consider. Furthermore, we identify the phase transition as a variant of the Berezinskii-Kosterlitz-Thouless (BKT) transition, which is known to exhibit critical properties not only at the transition point but also in the entire phase. This finding leads to the possibility that critical properties in natural languages may not require careful fine-tuning nor self-organized criticality, but is generically explained by the underlying connection between language structures and the BKT phases. From a statistical physics perspective, our paper captures a rare phenomenon of the BKT phase in a one-dimensional system; the BKT phase is widely studied and believed to exist only in two-dimensional systems.

*Introduction.*– Natural languages exhibit striking statistical regularities, such as Zipf’s law, which describes a power-law relationship between word frequencies and their rank [1]. Similarly, it has been shown that the number of bits of information provided by a symbol about another symbol drops roughly as a power law as a function of their distance [2]. These critical properties, observed across diverse languages, have inspired explanations rooted in statistical physics, drawing parallels between linguistic phenomena and phase transitions. For example, the scaling behavior inherent in Zipf’s law suggests underlying mechanisms that resemble those driving critical phenomena in physical systems [3].

Recent advances in generative language models, including large language models (LLMs) [4–7], have further highlighted intriguing connections between language and physics. Notably, studies have uncovered scaling laws and emergent capabilities in these models, which apparently become evident as the system size increases [8–10]. These findings have prompted the question of whether the statistical properties of natural languages and the behavior of their generative models can be understood

as manifestations of genuine phase transitions in physical terms.

These observed phenomena in LLMs, combined with the fact that they become apparent when some parameters of the system are large enough (network depth, width, training data set size, etc.), evoke parallels to phase transitions in the field of statistical physics. The fact that in critical (continuous) phase transitions many quantities such as the correlation function exhibit power-law scaling also fuels the approach to study these emergent phenomena in languages from a statistical physics perspective. The notion of phase transitions in the thermodynamic limit, i.e., in an idealized limit where some parameter governing the system size tends to infinity, enables us to study qualitative differences in the system in a rigorous way.

Such a formal qualitative study is essential because once we have a parameterized language model, it will always have a “trivial regime” corresponding to trivial distribution of characters/words/tokens, and an objectively defined hallmark of nontriviality – such as phase transitions – will be a theoretically powerful tool to distinguish meaningful sentences from those generated in the trivial regimes. Just as there is a clear and mathematically well-defined boundary between water and ice, the existence of a phase transition in language models could lead us to understand the intrinsic difference separating e.g., a

---

\*Electronic address: miyahara@ist.hokudai.ac.jp, hmiyahara512@gmail.com; corresponding author.

language-like structure that actually conveys information versus generated text that is just statistical gibberish.

A potential existence of a spin-glass-like phase transition in probabilistic context-free grammars (CFGs) has recently attracted attention [11, 12] (See Fig. 1(a) for a schematic diagram of CFGs). However, detailed analyses of CFGs have revealed the absence of such claimed phase transitions in some naturally assumed thermodynamic limit [13]. While consensus is yet to be reached on this matter [14, 15], it would be fair to say that numerical and analytical support for a true phase transition, i.e., a mathematically singular behavior in a clearly defined thermodynamic limit, is lacking. Furthermore, as probabilistic CFG is one of the simplest probabilistic models of natural language, this conundrum with the existence of phase transition naturally raises the question of how complex a natural language model needs to be in order to exhibit phase transitions.

Phase transition in statistical physics is a precisely defined mathematical concept that requires careful analysis. We provide a schematic figure of the types of phase transitions investigated in this paper in Fig. 1(b). In particular, to demonstrate phase transition one should be able to construct an *order parameter*, which is strictly zero in the disordered phase and is nonzero in the ordered phase, thus allowing a rigorous characterization of different phases in a system. This switch from zero to nonzero is inevitably accompanied by a mathematical singularity (a divergence or discontinuity in the derivative, etc) of the order parameter. Note that these features are only realized in the thermodynamic limit. In practice, one can only observe finite size systems and extrapolate the data to see consistency with the existence of phase transitions in the thermodynamic limit. In our paper, we will consider the relative frequencies of alphabets as the order parameter, and explore whether it shows a second-order phase transition, where the derivative of the order parameter has a singularity as a function of temperature. Temperature in the the context of a language model represents the probability with which a particular rule is applied in text generation.

There are, however, different types of second-order phase transitions. In a conventional one the critical behavior characterized by power-law scaling phenomena emerge only at the point of phase transition. That is, the system parameters have to be accurately tuned – so that the system is very close to the phase transition point – for any such scaling laws to be observed. Both LLMs and also natural languages, however, show robust scaling behaviors without requiring extensive fine tuning of parameters. This raises the possibility that for language models to exhibit phase transitions they might need to go through a different type of phase transition, referred to as the Berezinskii-Kosterlitz-Thouless (BKT) [16–20] transition. One of the most exceptional features of the BKT phase is that the system becomes critical throughout the entire phase, and not only at the transition point (See Fig. 1(b)). The presence of any BKT transition could

explain the robust presence of scaling laws in language models.

The BKT transition, however, is most commonly discussed in two-dimensional systems with continuous symmetries. On the other hand, since language models generate strings of text any reasonable physical modeling would lead to one-dimensional systems. While BKT transition is also realizable in long-range interacting one-dimensional systems, such one-dimensional phenomena are less studied and less well known. One method to determine whether a phase transition is BKT is to compute the kurtosis of the order parameter, which is referred to as the *Binder parameter* in the physics literature. The Binder parameter also nicely captures phase transitions – showing a singularity in its derivative – while being able to distinguish between different types of phases: it is strictly 0 in the disordered phase, and is exactly 1 in a conventionally ordered phase, while having a nontrivial value (between 0 and 1) at critical points where correlations have power-law decays; see Fig. 1(b). The Binder parameter becomes an especially powerful tool to study our language model since the model turns out to exhibit a type of the BKT phase.

In this study, we construct a probabilistic context-sensitive grammar (CSG), which unambiguously exhibits a phase transition. Our construction is based on the long-range interacting Potts model, and utilizes additional complexity CSGs possess from being one level higher in the Chomsky hierarchy [21, 22] compared to CFGs. Languages have a one-dimensional structure naturally associated to them: namely the direction from the beginning to the end of a sentence. Together with the observation that the degree of freedom in a sentence is essentially discrete (such as words or tokens), we focused our attention to the archetypal toy model in statistical physics with discrete degrees of freedom: the one-dimensional Potts model. We focus on the order parameter that captures the relative frequency of the letters or symbols in the string. We also compute the higher-order cumulants (variance and kurtosis) which corresponds to the susceptibility and Binder parameter in the physics perspective, and is the most widely used measure for detecting phase transitions. From the perspective of language models, e.g., the variance/susceptibility corresponds to how diverse the produced strings are, and therefore could be viewed as a measure of average nontriviality of the sentences. We compute the system-size dependence of the susceptibility and perform the finite-size scaling method [23–26], which allows us to confidently conclude the existence of a phase transition in the thermodynamic (infinite-size) limit. For example, we can observe a clear divergence of the susceptibility in the low-temperature BKT phase in our model, which indicates an entire parameter range where nontrivially correlated strings are produced.

In our numerical simulations, we first compute the system-size dependence of the quantity corresponding to magnetization. This quantifies how much a specific symbol is favored in the generating process of a sentence.

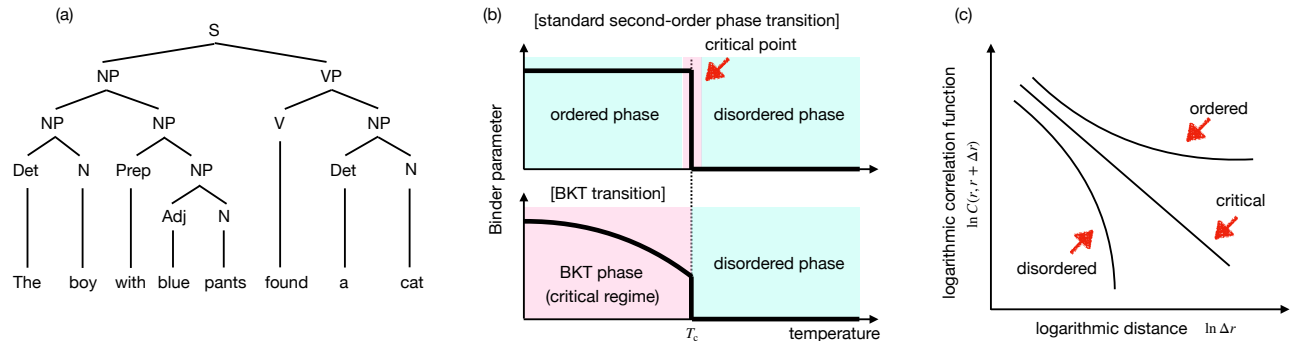


FIG. 1: (a) Schematic of a CFG. This diagram shows the syntactic structure of “The boy with blue pants found a cat.” Natural languages are, however, context sensitive and in this paper we define a simple context sensitive grammar (CSG) that demonstrates phase transition. (b) We consider the relative frequencies of letters or symbols in the alphabet – as captured by the net magnetization of the corresponding physical system – as an order parameter in our CSG. The Binder parameter, which is the normalized kurtosis of the underlying order parameter (see Eq. 8) can capture phase transition effectively, especially for one-dimensional models. A schematic of the Binder parameter is shown for the standard second-order phase transition (upper) and the BKT transition (lower). For the the BKT transition the the Binder parameter’s dependence on temperature – which determines the probability with which a rule is applied in the underlying CSG – does not become a step function in the thermodynamic limit. (c) Correlation functions for the disordered, critical, and ordered phases. When a system is critical, the correlation function shows a polynomial decay.

We also compute the corresponding susceptibility and the Binder parameter, which plays an important role to distinguish the standard second-order phase transition and the BKT transition [27, 28]. We then perform the finite-size scaling method to confirm the existence of phase transitions. In addition to these, we also investigate the correlation functions<sup>1</sup> between symbols [2]. These quantities play an essential role in discussing the scaling law in at least natural languages as the power-law scaling in correlation functions serves as the smoking gun for critical phase transitions in physics (See Fig. 1(c) for correlation functions)<sup>2</sup>.

It should be noted that the probabilistic CSG we have introduced is *not* a mere translation of the physical Potts model into a language model setting. The unique property of language models in general, absent in standard statistical mechanics models, is the increase in symbols over time, and there is an additional degree of freedom in how the symbols grow; see the parameters  $q, t$  and the specifics of the  $X \rightarrow YZ$  rule in Eq. 1b. *These properties of CSGs render the existence of a phase transition nontrivial*, and indeed we find that for certain settings of the language parameters, the phase transition can vanish. Furthermore, we compare CSGs with multiple alphabets to the one-dimensional long-range Potts model [29]. As

for phase transitions in one-dimensional models, it is well known that the Ising model – which is equivalent to the Potts model in the case of an alphabet of size two (i.e., two letters) – in one dimension shows no phase transition with short-range interactions but exhibits phase transitions with long-range interactions [30–38]. For the one-dimensional long-range Potts model with two-level spins ( $\sigma = \pm 1$ ), which is also known as the Ising model, it is known to exhibit an order at low temperatures and is known to undergo a BKT transition [19, 39–42]. Such BKT phase, however, is observed by considering  $s = 1$  in the exponent of the term that specifies a power-law decay in interaction with distance (see Eq. 4). In our language model we observe a BKT transition even when  $s = 0.9$ , which is far from the setting studied in Refs. [19, 40]. We also observe a BKT transition in our systems with multi-level spins, i.e., alphabets with  $K > 2$  letters. *We hypothesize that our language model where the system size grows in size following a set of probabilistic rules behaves differently from the physics models that inspired their conception and BKT transitions might be much more robust in our systems.*

*Language model.*– We here construct a probabilistic language model on the basis of the long range Potts model<sup>3</sup>. First of all, the generation process of a sentence begin with the start symbol, which is a nonterminal symbol. Until all the nonterminal symbols (lexical elements that specify the production rules constituting a formal grammar) in the sentence turn into terminal symbols (outputs of the production rules), a nontermi-

<sup>1</sup> In addition to the correlation function, we also compute mutual information in Sec. S-IV.

<sup>2</sup> Furthermore, we analyze the histogram of the magnetization and show typical configurations of symbols for parameters at which the histogram has a peak and relative frequencies of alphabets, which is often discussed in the context of natural language processing in Sec. S-IV.

<sup>3</sup> The details of our model are given in Sec. S-II.

nal symbol is uniformly randomly chosen and one of the following three processes is applied to it:

$$X \rightarrow x \quad (\text{probability: } qt), \quad (1a)$$

$$X \rightarrow YZ \quad (\text{probability: } q(1-t)), \quad (1b)$$

$$\alpha_- X \alpha_+ \rightarrow \alpha_- Y \alpha_+ \quad (\text{probability: } (1-q)), \quad (1c)$$

where uppercase and lowercase letters are nonterminal and terminal symbols, respectively, and  $\alpha_-$  and  $\alpha_+$  are strings. To take the thermodynamic limit, we set  $t = 0$ ; in other words, we do not consider Eq. (1a)<sup>4</sup>. For Eq. (1b), we consider two branching processes: (i)  $X \rightarrow YZ$  where  $Y$  and  $Z$  are uniformly randomly chosen and (ii)  $X \rightarrow XX$ . (In the main text, we focus on (i) and see Sec. S-IV for (ii).) Furthermore, when Eq. (1c) is chosen, the corresponding update is accepted with the following probability:

$$p = \min(1, e^{-\beta \Delta E}), \quad (2)$$

where

$$\Delta E := J \left( \sum_{\ell=1}^{\lfloor Nr_- \rfloor} \frac{\delta_{\sigma_0, \sigma_{-\ell}} - \delta_{\bar{\sigma}_0, \sigma_{-\ell}}}{\ell^{1+s}} + \sum_{\ell=1}^{\lfloor Nr_+ \rfloor} \frac{\delta_{\sigma_0 \sigma_\ell} - \delta_{\bar{\sigma}_0 \sigma_\ell}}{\ell^{1+s}} \right). \quad (3)$$

Here,  $r_+, r_- \in [0, 1]$  specify the range of interaction. Furthermore, we consider the open boundary condition; so terms beyond the boundary are ignored. Note that Eq. (2) is the acceptance rate of the Metropolis-Hastings algorithm [43–45] and Eq. (3) is the energy gap of the one-dimensional long-range Potts model with respect to a one-spin flip.

*Methods.*— We summarize the physical quantities of interest to discuss phase transitions<sup>5</sup>. First, we begin with the magnetization, which is the order parameter, reads

$$M := \|\mathbf{M}\|, \quad (4)$$

where  $\mathbf{M} \in \mathbb{R}^{K-1}$  is given by

$$\mathbf{M} := \frac{1}{N} \sum_{i=1}^N \mathbf{e}_{\sigma_i}. \quad (5)$$

Here,  $\{\mathbf{e}_k\}_{k=1}^K$  satisfy that  $\|\mathbf{e}_k\| = 1$  for  $k = 1, 2, \dots, K$ ,  $\mathbf{e}_k \cdot \mathbf{e}_l = \text{const.}$  for  $k \neq l$ , and  $\sum_{k=1}^K \mathbf{e}_k = \mathbf{0}$ <sup>6</sup>. Note that  $\|\mathbf{M}\| := \sqrt{\mathbf{M} \cdot \mathbf{M}}$ .

We then define the magnetic susceptibility by

$$\chi := N(\langle M^2 \rangle - \langle M \rangle^2). \quad (6)$$

For later convenience, we also define

$$\tilde{\chi} := N \langle M^2 \rangle. \quad (7)$$

As a well-used method to discern phase transitions, the Binder parameter is often used, and it reads

$$U := -\frac{K-1}{2} \left( \frac{\langle M^4 \rangle}{\langle M^2 \rangle^2} - \frac{K+1}{K-1} \right). \quad (8)$$

From the viewpoint of statistics, the Binder parameter, Eq. (8), is the normalized kurtosis, which becomes zero for the normal distribution. Thus, it can be used to distinguish the paramagnetic phase, in which the *generalized central limit theorem* empirically holds, and the ordered phase.

The correlation function is given by

$$\tilde{G}(i, j) := \langle \mathbf{e}_{\sigma_i} \cdot \mathbf{e}_{\sigma_j} \rangle. \quad (9)$$

It is well known that in a critical regime, the correlation function has a polynomial decay, while it has an exponential decay apart from a critical regime.

Finite-size scaling<sup>7</sup> is one of the most popular methods to discuss the existence of phase transitions. By applying the scaling assumption to  $\tilde{\chi}$ , Eq. (7), we obtain

$$\frac{\tilde{\chi}(T, L)}{L^{\frac{\gamma}{\nu}}} = \tilde{f}_{\tilde{\chi}}(L^{\frac{1}{\nu}} t). \quad (10)$$

Note that the scaling assumption implies the existence of a universal function  $\tilde{f}_A(\cdot)$  for any thermodynamic quantities  $A$ . We will confirm Eq. (10) via numerics.

*Numerical simulations.*— We show numerical simulations limiting ourselves to the case of  $K = 2$  and  $X \rightarrow YZ$ <sup>8</sup>. We run the Monte Carlo simulations  $80 \times 80$  times to compute expected values and standard errors.

We first plot the first 256 symbols of typical configurations of symbols in Fig. 2. Hereafter we investigate the statistical properties of these sentences.

In Fig. 3, we plot the temperature dependence of the magnetization, Eq. (4), the susceptibility, Eq. (6), and the Binder parameter, Eq. (8). First of all,  $k_B T \lesssim 1$ , the magnetization has a nonzero value ( $\langle M \rangle > 0$ ), and the system seems to be ordered. In the same regime, the susceptibility becomes not merely large but also divergent with respect to the system size for  $k_B T \lesssim 1$  unlike the second-order phase transition. In other words, the system is critical for a parameter regime of measure nonzero and this fact implies that the system is in the BKT phase. The Binder parameter also has a crossing point when the system size is varied; it also supports the existence of a phase transition.

In Fig. 4, we plot the correlation functions for different conditions. For a fixed system size, the correlation function look straight for  $k_B T \sim 1$  (See Fig. 4(upper)). Then, we turn our attention to the system-size

<sup>4</sup> This thermodynamic limit would be the simplest one while there should be different definitions of thermodynamic limits, which are beyond our scope.

<sup>5</sup> The details of the physical quantities computed in this paper are given in Sec. S-III.

<sup>6</sup> See Sec. S-III A for the derivation of  $\{\mathbf{e}_k\}_{k=1}^K$ .

<sup>7</sup> See Sec. S-III H for finite-size scaling.

<sup>8</sup> Numerical simulations for other setups are given in Sec. S-IV.

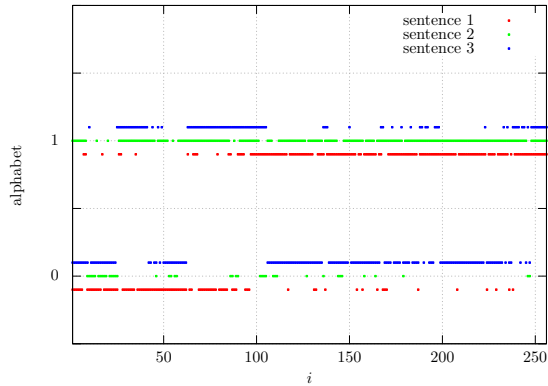


FIG. 2: Typical configurations of symbols for  $X \rightarrow YZ$ . We considered states of which magnetization lies between 0.0400 and 0.0600 at  $k_B T = 1.00$ . We set  $K = 2$ ,  $J = 1.0$ ,  $q = 10^{-2.0}$ ,  $t = 0$ ,  $s = 0.9$ , and  $r_- = r_+ = 0.25$ . We plot the first 256 symbols out of 4096.

dependence of the correlation function. As Fig. 4(lower) depicts, the correlation functions becomes straight for  $k_B T \lesssim 1$ .

In Fig. 5(upper), we draw the phase diagram of the CSG with  $K = 2$  and  $X \rightarrow YZ$ . In this phase diagram,  $T_c$ , below which the susceptibility is divergent with respect to the system size, is plotted by red dots and the fitting curve is computed via least square regression with a quadratic function. In other words, the susceptibility is not divergent with respect to the system size above  $T_c$ . We conduct finite-size scaling to  $\tilde{\chi}$  and plot the result in Fig. 5(middle). Finally, we show the  $q$ -dependence of the critical exponents  $\nu$  and  $\gamma$ . This figure shows that  $\nu$  increases with  $q$  but  $\gamma$  stays unchanged.

*Discussions.*— We here explore the numerical findings presented above, starting with the case of  $K = 2$ . The identified phase transition, reminiscent of the Ising model, entails the spontaneous breaking of  $\mathbb{Z}_2$  symmetry, presenting a unique form of phase transition distinct from those previously discussed in CSGs, as highlighted in prior works such as Refs. [11–13], and similar studies. Our investigation suggests that the phase transition phenomenon in CSGs is also fascinating compared to that of CFGs, which leads to the ongoing debate. Such a result implies that long-range interactions play a pivotal role in inducing a different type of a phase transition in language models.

Furthermore, the critical nature of the discovered phase transition is crucial. When arbitrarily constructing systems that undergoes phase transitions, it is common for transitions to be discontinuous (first-order). However, in such discontinuous transitions, the lack of non-trivial scaling laws makes them unsuitable for explaining phenomena like Zipf’s law, which is observed in natural languages.

It is important to note that the rules, such as Eq. (1b), involved in the studied statistical mechanics model are specific to language models and are not present in typ-

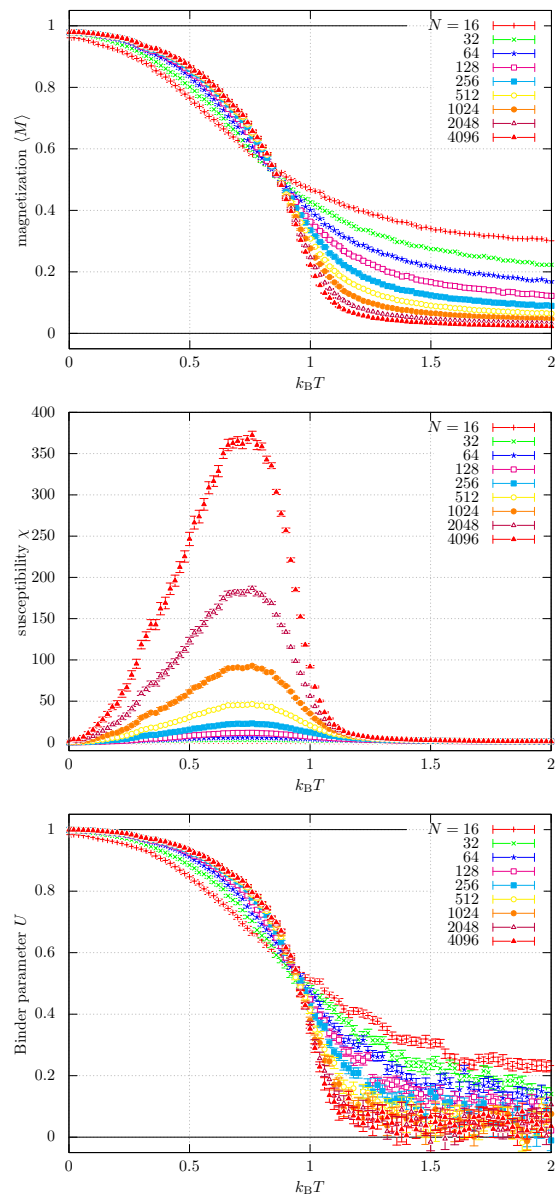


FIG. 3: Temperature dependence of (upper) the magnetization, Eq. (4), (middle) the susceptibility, Eq. (6), and (lower) the Binder parameter, Eq. (8), for  $X \rightarrow YZ$ . We set  $q = 10^{-2.0}$ . We also set  $K = 2$ ,  $J = 1.0$ ,  $t = 0$ ,  $s = 0.9$ , and  $r_- = r_+ = 0.25$ . The length of the generated sentence by the language model,  $N$ , was varied from 16 to 4096.

ical statistical mechanics models where the system does not grow over time. Therefore, the observed phase transition phenomenon in this study is not merely a repetition of calculations of the one-dimensional long-range Potts model in the context of natural language processing. The results of this study may offer new insights into the statistical mechanics of systems that spatially expand over time, beyond language-specific frameworks.

It is important to examine what occurs in the case of  $K > 2$  distinct alphabets, as this is a feature of any nat-

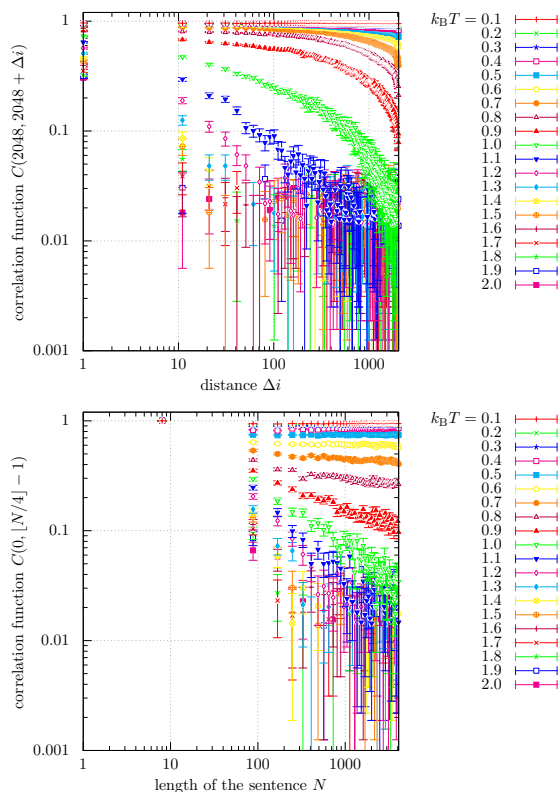


FIG. 4: Correlation functions, Eq. (9) (upper) with  $i = 2048$  and  $j = 2048 + \Delta i$  and (lower) with  $i = 0$  and  $j = \lfloor N/4 \rfloor - 1$  for  $X \rightarrow YZ$ . We set  $K = 2$ ,  $J = 1.0$ ,  $q = 10^{-2.0}$ ,  $t = 0$ ,  $s = 0.9$ , and  $r_- = r_+ = 0.25$ . Temperature  $k_B T$  was varied from 0.1 to 2.0.

ural language. Unlike the Potts model where  $K \geq 5$  exhibits a first-order phase transition, we observed the BKT transition in the CSGs with  $K = 10$ . However, its temperature dependence is heavily influenced by numerical conditions, and the unique processes specific to the CSG of interest, Eq. (1), contribute to a much richer phase diagram compared to conventional statistical-mechanical models.

We have also computed the correlation functions and mutual information for several numerical setups and observed the scaling laws. Due to the length-expanding nature of language models, there is some arbitrariness in the definition of correlation functions. Depending on this definition, the correlation functions exhibit power-law decay. This suggests the possibility of power laws occurring not only at the exact phase transition point, but potentially throughout an entire phase.

The relative frequencies of alphabets are often studied in natural language processing. For  $K = 10$  and  $q = 10^{-2.0}$ , we plot the relative frequencies of alphabets with typical configurations. Multiple symbols appear in sentences in the case of  $X \rightarrow YZ$ , while one or two symbols dominate sentences in the case of  $X \rightarrow XX$ . In natural languages, Zipf's law is believed to hold; thus, the case of  $X \rightarrow YZ$  seems to be more natural, though

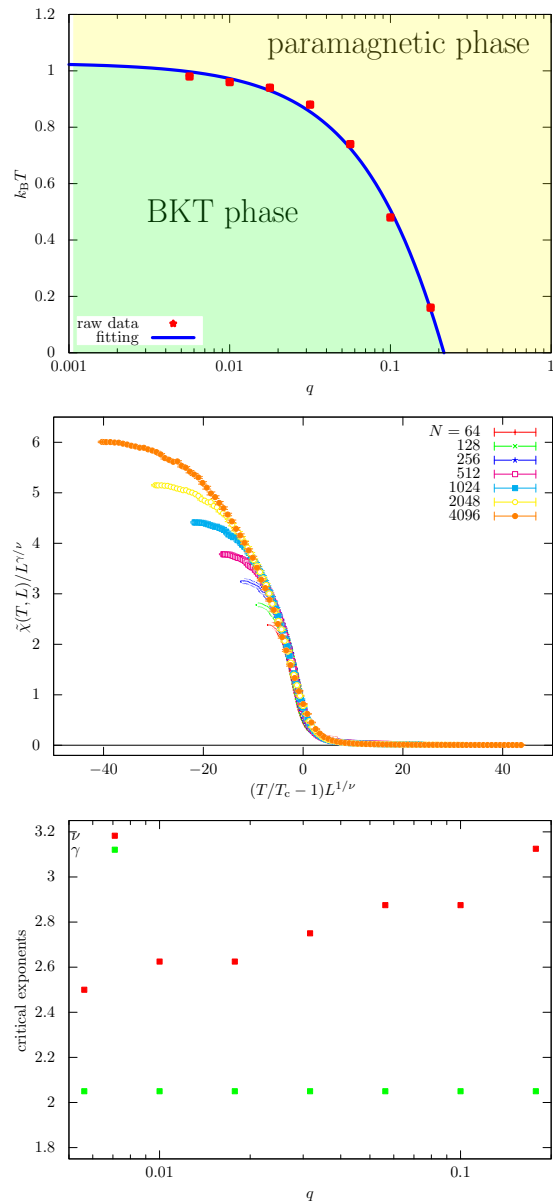


FIG. 5: (upper) Phase diagram of the CSG model investigated in this paper where the horizontal and vertical axes are the growth rate of a sentence  $q$  and critical temperature  $k_B T$ , respectively. We consider  $X \rightarrow YZ$  and set  $K = 2$ ,  $J = 1.0$ ,  $t = 0$ ,  $s = 0.9$ , and  $r_- = r_+ = 0.25$ . (middle) Finite-size scaling of  $\tilde{\chi}$  at  $q = 10^{-2.0}$ . We set  $T_c = 0.960$ ,  $\nu = 2.50$ , and  $\gamma = 2.05$ , where the values of  $\nu$  and  $\gamma$  are determined such that the scaling assumption holds. We varied  $N = 64, 128, 256, 512, 1024, 2048, 4096$ . (lower)  $q$ -dependence of the critical exponents  $\nu$  and  $\gamma$ .

the phenomenon observed in the case of  $X \rightarrow XX$  looks quite similar to that of the first-order phase transition. However, further investigation may be required to reach a definitive conclusion, as there are several different branching processes, including those that exist between  $X \rightarrow YZ$  and  $X \rightarrow XX$ .

In finite-size scaling, we determined the critical expo-

nents such the scaling assumption holds. It is important to note that the existence of such values is non-trivial; there is no universal function in general. In Ref. [37], the critical exponents of the one-dimensional long-range Ising model is reported, but our observation is that the scaling assumption does not hold for these quantities. Furthermore,  $\gamma$  and  $\nu$  do not depend on the choice between  $X \rightarrow YZ$  and  $X \rightarrow XX$ ; on the other hand, they depend on  $q$  and  $K$ . The phase diagrams heavily depend on the choice between  $X \rightarrow YZ$  and  $X \rightarrow XX$ , making the independence of  $\gamma$  and  $\nu$  from these choices an interesting feature. The fact that  $\gamma$  and  $\nu$  depend on  $K$  seems to be natural since the number of states or flavors often affect renormalization flows. Contrary to the choice between  $X \rightarrow YZ$  and  $X \rightarrow XX$ ,  $\gamma$  and  $\nu$  depend on  $q$ , which is a newly introduced parameter that controls the growth rate of a sentence.

The reader may find that the above discussions seem to contradict common understanding regarding the BKT transition. Typically, the BKT transition is studied within the context of the  $XY$  model, where it is believed that  $\mathbb{Z}_2$  spontaneous symmetry breaking does not occur [16–18]. In contrast, the one-dimensional long-range Ising model is known to exhibit  $\mathbb{Z}_2$  spontaneous symmetry breaking [46–50] alongside the BKT transition [19, 40]. In this sense, our study sheds light on the *unconventional* BKT transition and posits that it may capture the nature of language models.

Additionally, in deep learning models for natural language processing, attention mechanisms are considered crucial [51]. These attention mechanisms facilitate long-range interactions, aligning with the results of our study, which suggest that long-range interactions play a role in stabilizing phase transitions in language models. More recently, the possibility of a mirage of the emergent ability of LLMs was pointed out in Ref. [52]; so a similar investigation of neural language models and LLMs is one of the most important future directions.

*Conclusions.*— In this study, we have constructed CSGs by combining CFGs with the one-dimensional long-range Potts model, and we numerically demonstrated the presence and absence of phase transitions depending on numerical conditions. Moreover, we unveiled nontrivial phase transition phenomena specific to language model rules. In the future, it will be intriguing to explore whether more nontrivial phase transitions, as discussed in Refs. [11, 13], can be realized in CSGs or their probabilistic extension models, akin to the transitions observed in this study. Additionally, by considering more realistic language models, we aim to elucidate the scaling laws

observed in LLMs and the mechanisms behind emergent language capabilities.

Indeed, our study has shed light on the significance of long-range interactions in the phase transition of language models. However, the precise relationship with mechanisms such as attention mechanisms remains ambiguous. Future research endeavors will seek to elucidate the behavior of attention mechanisms in the long-range limit and establish connections between long-range interactions, attention mechanisms, phase transitions, scaling laws, and the emergence of language capabilities.

It is worth noting that Ref. [53] discusses a phase transition in a neural language model, which is indeed intriguing. However, the approach differs from ours; while our work focuses on identifying the minimal language model that exhibits phase transitions, Ref. [53] directly investigates a neural language model.

### Acknowledgments

H.M. thanks Koji Hukushima, Kai Nakaishi, Sho Yokoi, Ryo Ueda, Tatsuki Kuribayashi, Takashi Mori, Masahito Mochizuki, Yusuke Miyajima, and Masaharu Yoshioka for fruitful discussions. J.T. thanks Yoshihiko Nishikawa, K. Nakaishi, K. Hukushima, S. Yokoi, R. Ueda, and T. Kuribayashi for insightful discussions too. H.M. was supported by JSPS KAKENHI Grant Number 23H04489.

### Author contributions

H.M. conceived the original idea. H.M. and J.T. designed research. Y.T. and H.M. performed numerical simulations. All the authors discussed the results. H.M., J.T., and V.R. wrote the paper.

### Competing interests

The authors declare no competing financial interests.

### Data availability

We will provide all the numerical codes and plot files upon request.

- 
- [1] S. T. Piantadosi, *Psychonomic bulletin & review* **21**, 1112 (2014).  
 [2] H. W. Lin and M. Tegmark, *Entropy* **19** (2017), ISSN 1099-4300, URL <https://www.mdpi.com/1099-4300/19/7/299>.

- [3] M. Simkin and V. Roychowdhury, *Physics Reports* **502**, 1 (2011), ISSN 0370-1573, URL <https://www.sciencedirect.com/science/article/pii/S0370157310003339>.  
 [4] OpenAI, *Hello GPT-4o* (2022), URL <https://openai.com>.

- com/index/chatgpt/.
- [5] S. Pichai and D. Hassabis, *Introducing gemini: our largest and most capable ai model* (2023), URL <https://blog.google/technology/ai/google-gemini-ai/>.
  - [6] H. Naveed, A. U. Khan, S. Qiu, M. Saqib, S. Anwar, M. Usman, N. Akhtar, N. Barnes, and A. Mian, arXiv preprint arXiv:2307.06435 (2023).
  - [7] M. U. Hadi, Q. Al Tashi, A. Shah, R. Qureshi, A. Muneer, M. Irfan, A. Zafar, M. B. Shaikh, N. Akhtar, J. Wu, et al., Authorea Preprints (2024).
  - [8] J. Kaplan, S. McCandlish, T. Henighan, T. B. Brown, B. Chess, R. Child, S. Gray, A. Radford, J. Wu, and D. Amodei, arXiv preprint arXiv:2001.08361 (2020).
  - [9] J. Wei, Y. Tay, R. Bommasani, C. Raffel, B. Zoph, S. Borgeaud, D. Yogatama, M. Bosma, D. Zhou, D. Metzler, et al., arXiv preprint arXiv:2206.07682 (2022).
  - [10] A. Chen, R. Schwartz-Ziv, K. Cho, M. L. Leavitt, and N. Saphra, arXiv preprint arXiv:2309.07311 (2023).
  - [11] E. DeGiuli, Phys. Rev. Lett. **122**, 128301 (2019), URL <https://link.aps.org/doi/10.1103/PhysRevLett.122.128301>.
  - [12] E. D. Giuli, Journal of Physics A: Mathematical and Theoretical **52**, 504001 (2019), URL <https://doi.org/10.1088/1751-8121/ab293c>.
  - [13] K. Nakaishi and K. Hukushima, Phys. Rev. Research **4**, 023156 (2022), URL <https://link.aps.org/doi/10.1103/PhysRevResearch.4.023156>.
  - [14] F. Lalegani and E. De Giuli, arXiv preprint arXiv:2309.14913 (2023).
  - [15] K. Nakaishi and K. Hukushima, arXiv preprint arXiv:2402.07113 (2024).
  - [16] V. Berezinskii, Sov. Phys. JETP **32**, 493 (1971).
  - [17] V. Berezinskii, Sov. Phys. JETP **34**, 610 (1972).
  - [18] J. M. Kosterlitz and D. J. Thouless, Journal of Physics C: Solid State Physics **6**, 1181 (1973), URL <https://dx.doi.org/10.1088/0022-3719/6/7/010>.
  - [19] J. M. Kosterlitz, Reports on Progress in Physics **79**, 026001 (2016), URL <https://dx.doi.org/10.1088/0034-4885/79/2/026001>.
  - [20] J. M. Kosterlitz, Journal of Physics C: Solid State Physics **7**, 1046 (1974), URL <https://dx.doi.org/10.1088/0022-3719/7/6/005>.
  - [21] G. Jäger and J. Rogers, Philosophical Transactions of the Royal Society B: Biological Sciences **367**, 1956 (2012).
  - [22] G. Delétang, A. Ruoss, J. Grau-Moya, T. Genewein, L. K. Wenliang, E. Catt, C. Cundy, M. Hutter, S. Legg, J. Veness, et al., arXiv preprint arXiv:2207.02098 (2022).
  - [23] V. Ardourel and S. Bangu, Studies in History and Philosophy of Science **100**, 99 (2023), ISSN 0039-3681, URL <https://www.sciencedirect.com/science/article/pii/S0039368123000900>.
  - [24] Y.-D. Hsieh, Y.-J. Kao, and A. W. Sandvik, Journal of Statistical Mechanics: Theory and Experiment **2013**, P09001 (2013), URL <https://dx.doi.org/10.1088/1742-5468/2013/09/P09001>.
  - [25] Z. Zuo, S. Yin, X. Cao, and F. Zhong, Phys. Rev. B **104**, 214108 (2021), URL <https://link.aps.org/doi/10.1103/PhysRevB.104.214108>.
  - [26] H. Ueda, K. Okunishi, K. Harada, R. Krčmár, A. Gendiar, S. Yunoki, and T. Nishino, Phys. Rev. E **101**, 062111 (2020), URL <https://link.aps.org/doi/10.1103/PhysRevE.101.062111>.
  - [27] M. Hasenbusch, Journal of Statistical Mechanics: Theory and Experiment **2008**, P08003 (2008), URL <https://dx.doi.org/10.1088/1742-5468/2008/08/P08003>.
  - [28] L. M. Tuan, T. T. Long, D. X. Nui, P. T. Minh, N. D. Trung Kien, and D. X. Viet, Phys. Rev. E **106**, 034138 (2022), URL <https://link.aps.org/doi/10.1103/PhysRevE.106.034138>.
  - [29] E. Bayong, H. T. Diep, and V. Dotsenko, Phys. Rev. Lett. **83**, 14 (1999), URL <https://link.aps.org/doi/10.1103/PhysRevLett.83.14>.
  - [30] F. J. Dyson, Matematika **16**, 137 (1972).
  - [31] J. Fröhlich and T. Spencer (1982).
  - [32] F. J. Dyson, Matematika **16**, 113 (1972).
  - [33] F. J. Dyson, Communications in Mathematical Physics **21**, 269 (1971).
  - [34] D. J. Thouless, Phys. Rev. **187**, 732 (1969), URL <https://link.aps.org/doi/10.1103/PhysRev.187.732>.
  - [35] Y. Chang, L. Sun, and X. Cai, Phys. Rev. E **76**, 021101 (2007), URL <https://link.aps.org/doi/10.1103/PhysRevE.76.021101>.
  - [36] J. Martínez-Herrera, O. Rodríguez-López, and M. Solís, Physica A: Statistical Mechanics and its Applications **596**, 127136 (2022), ISSN 0378-4371, URL <https://www.sciencedirect.com/science/article/pii/S0378437122001534>.
  - [37] Y. Tomita, Journal of the Physical Society of Japan **78**, 014002 (2009), <https://doi.org/10.1143/JPSJ.78.014002>, URL <https://doi.org/10.1143/JPSJ.78.014002>.
  - [38] Y. Chang, L. Sun, and X. Cai, Phys. Rev. E **76**, 021101 (2007), URL <https://link.aps.org/doi/10.1103/PhysRevE.76.021101>.
  - [39] P. W. Anderson and G. Yuval, Journal of Physics C: Solid State Physics **4**, 607 (1971), URL <https://dx.doi.org/10.1088/0022-3719/4/5/011>.
  - [40] J. M. Kosterlitz, Phys. Rev. Lett. **37**, 1577 (1976), URL <https://link.aps.org/doi/10.1103/PhysRevLett.37.1577>.
  - [41] M. Aizenman and R. Fernández, Letters in Mathematical Physics **16**, 39 (1988).
  - [42] M. Aizenman, J. T. Chayes, L. Chayes, and C. M. Newman, Journal of Statistical Physics **50**, 1 (1988).
  - [43] D. Landau and K. Binder, *A Guide to Monte Carlo Simulations in Statistical Physics* (Cambridge University Press, 2021), ISBN 9781108490146, URL <https://books.google.co.jp/books?id=WW8yEAAAQBAJ>.
  - [44] J. Binney, N. Dowrick, A. Fisher, and M. Newman, *The Theory of Critical Phenomena: An Introduction to the Renormalization Group* (Clarendon Press, 1992), ISBN 9780191660566, URL <https://books.google.co.jp/books?id=BCOQDwAAQBAJ>.
  - [45] M. Newman and G. Barkema, *Monte Carlo Methods in Statistical Physics* (Clarendon Press, 1999), ISBN 9780198517962, URL <https://books.google.co.jp/books?id=KKL2nQEACAAJ>.
  - [46] P. W. Anderson and G. Yuval, Phys. Rev. Lett. **23**, 89 (1969), URL <https://link.aps.org/doi/10.1103/PhysRevLett.23.89>.
  - [47] G. Yuval and P. W. Anderson, Phys. Rev. B **1**, 1522 (1970), URL <https://link.aps.org/doi/10.1103/PhysRevB.1.1522>.
  - [48] P. W. Anderson, G. Yuval, and D. R. Hamann, Phys. Rev. B **1**, 4464 (1970), URL <https://link.aps.org/doi/10.1103/PhysRevB.1.4464>.
  - [49] D. R. Hamann, Phys. Rev. Lett. **23**, 95 (1969), URL <https://link.aps.org/doi/10.1103/PhysRevLett.23.95>.

- [50] P. W. Anderson and G. Yuval, *Journal of Physics C: Solid State Physics* **4**, 607 (1971), URL <https://dx.doi.org/10.1088/0022-3719/4/5/011>.
- [51] A. Vaswani, N. Shazeer, N. Parmar, J. Uszkoreit, L. Jones, A. N. Gomez, L. Kaiser, and I. Polosukhin, *Advances in neural information processing systems* **30** (2017).
- [52] R. Schaeffer, B. Miranda, and S. Koyejo, arXiv preprint arXiv:2304.15004 (2023).
- [53] H. Cui, F. Behrens, F. Krzakala, and L. Zdeborová, arXiv preprint arXiv:2402.03902 (2024).

**Supplemental Information**  
**– First numerical observation of the Berezinskii-Kosterlitz-Thouless transition in language models –**

Yuma Toji and Hideyuki Miyahara\*  
*Graduate School of Information Science and Technology,  
Hokkaido University, Sapporo, Hokkaido 060-0814, Japan*

Jun Takahashi  
*Institute for Solid State Physics, The University of Tokyo,  
5-1-5 Kashiwanoha, Kashiwa, Chiba 277-8581, Japan*

Vwani Roychowdhury  
*Henry Samueli School of Engineering and Applied Science,  
University of California, Los Angeles, California 90095*  
(Dated: December 3, 2024)

**Contents**

<b>S-I. Introduction</b>	2
<b>S-II. Language model</b>	2
A. Proposed Model	2
B. One-dimensional long-range Potts model	3
C. One-dimensional long-range Ising model	3
D. Context-dependency	4
<b>S-III. Methods: physical quantities for discussing phase transitions and finite-size scaling</b>	4
A. Magnetization	4
B. Derivation of Eq. (S-3.3)	5
C. Susceptibility	6
D. Binder parameter	6
E. Correlation function	6
F. Mutual information	7
G. Histogram of the magnetization	7
H. Finite-size scaling	7
<b>S-IV. Numerical simulations</b>	8
A. Case where 2 symbols are increasing at random: $K = 2$ and $X \rightarrow YZ$	8
1. Magnetization, susceptibility, and Binder parameter	8
2. Correlation functions, mutual information, and histogram of magnetization for $q = 10^{-2.0}$	9
3. Correlation functions, mutual information, and histogram of magnetization for $q = 10^{-0.5}$	10
4. System-size dependence of the magnetization, the susceptibilities, and the Binder parameter	10
5. Phase diagram, finite-size scaling, and $q$ -dependence of critical exponents	10
B. Case where 2 symbols duplicates: $K = 2$ and $X \rightarrow XX$	11
1. Magnetization, susceptibility, and Binder parameter	11
2. Correlation functions, mutual information, and histogram of magnetization for $q = 10^{-2.0}$	12
3. Correlation functions, mutual information, and histogram of magnetization for $q = 10^{-0.5}$	12
4. System-size dependence of the magnetization, the susceptibilities, and the Binder parameter	13
5. Phase diagram, finite-size scaling, and $q$ -dependence of critical exponents	13
C. Case where 10 symbols are increasing at random: $K = 10$ and $X \rightarrow YZ$	13

---

\*Electronic address: miyahara@ist.hokudai.ac.jp, hmiyahara512@gmail.com; corresponding author.

1. Magnetization, susceptibility, and Binder parameter	14
2. Correlation functions, mutual information, and histogram of magnetization for $q = 10^{-2.0}$	14
3. Correlation functions, mutual information, and histogram of magnetization for $q = 10^{-0.5}$	15
4. System-size dependence of the magnetization, the susceptibilities, and the Binder parameter	15
5. Phase diagram, finite-size scaling, and $q$ -dependence of critical exponents	15
6. Configurations and relative frequencies for $q = 10^{-2.0}$	16
D. Case where 10 symbols duplicates: $K = 10$ and $X \rightarrow XX$	16
1. Magnetization, susceptibility, and Binder parameter	17
2. Correlation functions, mutual information, and histogram of magnetization for $q = 10^{-2.0}$	17
3. Correlation functions, mutual information, and histogram of magnetization for $q = 10^{-0.5}$	18
4. System-size dependence of the magnetization, the susceptibilities, and the Binder parameter	18
5. Phase diagram, finite-size scaling, and $q$ -dependence of critical exponents	18
6. Configurations and relative frequencies for $q = 10^{-2.0}$	19
<b>References</b>	<b>34</b>

## S-I. INTRODUCTION

This material provides the supplemental information for the paper entitled “First numerical observation of the Berezinskii-Kosterlitz-Thouless transition in language models”. The remainder of this paper is organized as follows. In Sec. S-II, we formulate the problem setting of this study. Section S-III demonstrates some physical quantities computed in this paper. Section S-IV presents supporting numerical simulations.

## S-II. LANGUAGE MODEL

This section outlines the model under consideration in this study. With regards to the model, particular emphasis is placed on explaining the interactions between symbols. As the interaction between symbols, we consider the one-dimensional Potts model with long-range interaction and construct a new CSG. Note that the Potts model is identical to the Ising model when the number of states that each spin has is two. Finally, we explain the context-dependency of the constructed language model.

### A. Proposed Model

In this study, we consider a language model that significantly simplifies natural language as a model with  $K$  alphabets [1–6]. In the language model, we begin with a randomly chosen symbol, which is a nonterminal symbol. Then, a symbol in the sentence is first chosen uniformly at random and one of the following three generation rules is applied to the symbol:

$$X \rightarrow x \quad (\text{probability: } qt), \quad (\text{S-2.1a})$$

$$X \rightarrow YZ \quad (\text{probability: } q(1-t)), \quad (\text{S-2.1b})$$

$$\alpha_- X \alpha_+ \rightarrow \alpha_- Y \alpha_+ \quad (\text{probability: } (1-q)). \quad (\text{S-2.1c})$$

Here, uppercase letters  $X$ ,  $Y$ , and  $Z$  represent non-terminal symbols, taking values  $A_1, A_2, \dots, A_K$ . Lowercase letters  $x$ ,  $y$ , and  $z$  represent terminal symbols, taking values  $a_1, a_2, \dots, a_K$ . Firstly, Eq. (S-2.1a) represents rules where non-terminal symbols correspond to their respective terminal symbols. Secondly, Eq. (S-2.1b) represents rules where a non-terminal symbol is replaced by two non-terminal symbols. Lastly, Eq. (S-2.1c) introduces context-dependency to non-terminal symbols, rewriting them based on the context  $\alpha_-$  and  $\alpha_+$ , which are strings before and after the symbol of interest, respectively. Furthermore,  $Y$  in Eq. (S-2.1c), called the proposed sample in the Monte Carlo (MC) method, is chosen from a probability distribution that satisfies the detailed balance condition. In this paper, we run the Metropolis-Hastings algorithm to determine if this update is executed or not. We describe the details later.

While there may be room for discussion regarding the extent of context-dependency in natural languages, we adopt CSGs with a focus on strong context access in modern neural language models. It is worth noting that excluding Eq. (S-2.1c) leads to a CFG, aligning with models discussed in previous studies [1–6]. The probabilities of adopting rules in Eqs. (S-2.1a), (S-2.1b), and (S-2.1c) are denoted as  $qt$ ,  $q(1-t)$ , and  $1-q$ , respectively. The parameter  $t \rightarrow 0$  represents the limit where non-terminal symbols do not appear, serving as the most straightforward thermodynamic

limit  $N \rightarrow \infty$ , and this limit enables us to discuss phase transitions. Then, in this paper, we focus on this limit for simplicity.

### B. One-dimensional long-range Potts model

In Refs. [7–15], the phase transition in the following one-dimensional long-range Potts model <sup>1</sup> is discussed [16]:

$$H = - \sum_{\substack{i,j=1,2,\dots,N, \\ i < j}} J_{i,j} \delta_{\sigma_i, \sigma_j}, \quad (\text{S-2.2})$$

where

$$J_{i,j} = \begin{cases} \frac{J}{|i-j|^{1+s}} & (j-i \in [Nr_-, Nr_+]), \\ 0 & (\text{otherwise}). \end{cases} \quad (\text{S-2.3})$$

Here  $r_+, r_- \in [0, 1]$  are parameters that specify the range of interaction. Note that Eq. (S-2.2) is referred to as the ferromagnetic model because symbols are more likely to have the same state for  $J \gg 0$ . Additionally, when  $X_j = A_k, a_k$  for  $k = 1, 2, \dots, K$ ,  $\sigma_j$  is defined as

$$\sigma_j = k. \quad (\text{S-2.4})$$

For the pedagogical purpose, we describe the case of  $K = 2$  in Sec. S-II C.

### C. One-dimensional long-range Ising model

In the literature,  $\sigma_i = \pm 1$  for  $K = 2$ , i.e., the Ising model; then, we follow the notation in this subsection. Eq. (S-2.2) with  $K = 2$  reads

$$H = -\frac{1}{2} \sum_{\substack{i,j=1,2,\dots,N, \\ i < j}} J_{i,j} \sigma_i \sigma_j, \quad (\text{S-2.5})$$

where  $h := h_1 = -h_2$ . Eq. (S-2.4) is transformed into

$$\sigma_j := \begin{cases} 1 & (X_j = A_1, a_1), \\ -1 & (X_j = A_2, a_2). \end{cases} \quad (\text{S-2.6})$$

Eq. (S-2.10) for  $\sigma_0 \rightarrow \tilde{\sigma}_0 = -\sigma_0$  becomes

$$\Delta E := -\frac{J}{2} \left( \sum_{\ell=1}^{\lfloor Nr_- \rfloor} \frac{(\tilde{\sigma}_0 - \sigma_0) \sigma_{-\ell}}{\ell^{1+s}} + \sum_{\ell=1}^{\lfloor Nr_+ \rfloor} \frac{(\tilde{\sigma}_0 - \sigma_0) \sigma_{\ell}}{\ell^{1+s}} \right) \quad (\text{S-2.7})$$

$$= J \left( \sum_{\ell=1}^{\lfloor Nr_- \rfloor} \frac{\sigma_0 \sigma_{-\ell}}{\ell^{1+s}} + \sum_{\ell=1}^{\lfloor Nr_+ \rfloor} \frac{\sigma_0 \sigma_{\ell}}{\ell^{1+s}} \right). \quad (\text{S-2.8})$$

We review the studies on phase transitions of the one-dimensional long-range Ising model (the one-dimensional long-range Potts model with  $K = 2$ ) (S-2.2). For this model, phase transitions happen for  $s \in (0, 1)$  while phase transitions do not exist for  $s > 1$  [7, 9, 10, 13, 14]. In Ref. [8], the existence of a phase transition for  $s = 1$  was reported. Furthermore, When  $s = 1$ , it is known that the BKT transition happens [17, 18].

There are numerous studies on critical exponents for various  $s$  [19]. For  $s \in (0, 0.5)$ , it has been reported that the phase transition follows the mean-field approximation and exhibits a jump in the specific heat [20]. Additionally, the critical exponent is noted to be independent of temperature in this range [21]. For  $s \in (0.5, 1.0)$ , a sharp peak in the specific heat suggests a phase transition distinct from that predicted by the mean-field approximation [20]. In this paper, we consider  $s$  within this range for simplicity. Furthermore, at  $s = 1$ , there is a jump in magnetization [10, 11, 22]. It is also worth noting that an effective MC method was proposed in Ref. [23].

---

<sup>1</sup> This model is called the Potts model when  $K$  is 2.

### D. Context-dependency

Let us elaborate on Eq. (S-2.1c). Let  $N$  be the length of the entire string, and define  $\alpha_- := X_{-\lfloor Nr_- \rfloor} X_{-(\lfloor Nr_- \rfloor - 1)} \dots X_{-2} X_{-1}$  and  $\alpha_+ := X_1 X_2 \dots X_{\lfloor Nr_+ \rfloor - 1} X_{\lfloor Nr_+ \rfloor}$ . Here,  $X$  represents any alphabet, and the subscript values denote the relative positions with respect to  $A_1, A_2, \dots, A_K$  in Eq. (S-2.1c). The floor function  $\lfloor x \rfloor$  indicates the greatest integer that is equal to or smaller than  $x \in \mathbb{R}$ , and  $r_-$  and  $r_+$  are parameters corresponding to the interaction range of the one-dimensional long-range Potts model.

Let  $i = 0$  be the location of  $X$ . Motivated by the Metropolis-Hastings algorithm, when Eq. (S-2.1c) is chosen, symbols are changed with the following probability:

$$p = \min(1, e^{-\beta \Delta E}), \quad (\text{S-2.9})$$

where  $\Delta E$  for  $\sigma_0 \rightarrow \tilde{\sigma}_0$  is defined as:

$$\Delta E := J \left( \sum_{\ell=1}^{\lfloor Nr_- \rfloor} \frac{\delta_{\sigma_0, \sigma_{-\ell}} - \delta_{\tilde{\sigma}_0, \sigma_{-\ell}}}{\ell^{1+s}} + \sum_{\ell=1}^{\lfloor Nr_+ \rfloor} \frac{\delta_{\sigma_0 \sigma_\ell} - \delta_{\tilde{\sigma}_0 \sigma_\ell}}{\ell^{1+s}} \right). \quad (\text{S-2.10})$$

Note that Eq. (S-2.10) is computed from Eq. (S-2.2):  $\Delta E = \tilde{H} - H$ . Here  $\beta := 1/(k_B T)$ .

According to Eq. (S-2.9), symbols are more likely to flip when  $\Delta E$  is small. Furthermore, from Eq. (S-2.10),  $\Delta E$  decreases when the numerator of the first and second terms of the right-hand side of Eq. (S-2.10) take negative values. Considering Eq. (S-2.4), this means symbols flip when the surrounding symbols are of a different type. The parameter  $k_B T$  controls the tendency of the same symbols to align and corresponds to the strength of the desire in statistical mechanics to align with the absolute temperature.

Eq. (S-2.10) is termed long-range interaction due to the power-law decay ( $1/\ell^{1+s}$ ) of interactions between symbols. The parameter  $s$  determines the strength of the power-law decay, and in this paper, we fix  $s = 0.9$ . In summary, the rule in Eq. (S-2.1c) is statistically equivalent to the Metropolis-Hastings algorithm for flipping a single symbol in the one-dimensional long-range Potts model, as applied in MC simulations.

### S-III. METHODS: PHYSICAL QUANTITIES FOR DISCUSSING PHASE TRANSITIONS AND FINITE-SIZE SCALING

Phase transitions are discerned through the singularity of order parameters, which represent the expectation value of certain random variables. In models like the Potts model, magnetization, denoting the ratio of up and down spins, is commonly employed as an order parameter. Subsequently, we examine the second-order moment of the random variable, known as susceptibility. At critical points, susceptibility typically diverges, making it crucial to observe its behavior to confirm phase transitions. Moreover, the Binder parameter, akin to the normalized version of kurtosis, plays a crucial role in discussions of phase transitions. According to a generalized version of the *generalized central limit theorem*, the Binder parameter is one below the critical temperature and zero above it. Furthermore, in the case of second-order phase transitions, lines depicting the temperature dependence of the Binder parameter for fixed system sizes intersect at the critical temperature.

To explore the scaling law, which is known to apply at critical points, we also compute the correlation functions and mutual information. It is important to note that due to the inherent growth property of language models, there is some arbitrariness in defining the correlation functions and mutual information.

At the end of this section, we review the finite-size scaling method, which is a powerful method based on the scaling assumption to discuss and quantify phase transitions. In particular, critical exponents are used to classify phase transitions into universality classes.

#### A. Magnetization

Although this study does not deal with magnetic materials, an order parameter similar to the Potts model can be defined when considering two symbols. We term this order parameter ‘‘magnetization’’ and define it as follows:

$$M := \|\mathbf{M}\|, \quad (\text{S-3.1})$$

where  $\mathbf{M} \in \mathbb{R}^{K-1}$  is given by

$$\mathbf{M} := \frac{1}{N} \sum_{i=1}^N e_{\sigma_i}. \quad (\text{S-3.2})$$

---

**ALGO. 1:** Construction of  $\{\mathbf{e}_k\}_{k=1}^K$  in Eq. (S-3.1).

---

```

1 set  $\mathbf{e}_1 := [1, 0, \dots, 0]^\top$ 
2 for  $k = 2, 3, 4, \dots, K$  do
3   initialize  $\mathbf{e}_k := [0, 0, \dots, 0]^\top$ 
4   for  $l = 1, 2, 3, \dots, k-1$  do
5      $[e_k]_l = -\frac{1}{K-l}[e_l]$ 
6    $[e_k]_k = \sqrt{1 - \sum_{l=1}^k ([e_k]_l)^2}$ 

```

---

Note that  $\|\mathbf{M}\| := \sqrt{\mathbf{M} \cdot \mathbf{M}}$ . The construction of  $\{\mathbf{e}_k\}_{k=1}^K$  in Eq. (S-3.1) is shown in Algo. 1. Due to its construction, Algo. 1,  $\{\mathbf{e}_k\}_{k=1}^K$  satisfy that  $\|\mathbf{e}_k\| = 1$  for  $k = 1, 2, \dots, K$ ,  $\mathbf{e}_k \cdot \mathbf{e}_l = \text{const.}$  for  $k \neq l$ , and  $\sum_{k=1}^K \mathbf{e}_k = \mathbf{0}$ . Then the  $l$ -th element of  $\{\mathbf{e}_k\}_{k=1}^K$  is computed as

$$[e_k]_l := \begin{cases} \sqrt{\frac{K(K-k)}{(K-1)(K-k+1)}} & (k = l), \\ -\sqrt{\frac{K}{(K-1)(K-l)(K-l+1)}} & (k > l), \\ 0 & (k < l). \end{cases} \quad (\text{S-3.3})$$

The detailed derivation of Eq. (S-3.3) is shown in Sec. S-III B. Note that  $\langle \mathbf{M} \rangle = \mathbf{0}$  due to the construction of  $\{\mathbf{e}_k\}_{k=1}^K$ .

Let us delve into the meaning of  $M$ , as defined in Eq. (S-3.1); it signifies the degree of frequency bias among alphabets  $A_1, A_2, \dots, A_K$ . In the subsequent analysis, by observing the variations of  $M$ , Eq. (S-3.1), with respect to the independent variable temperature  $k_B T$ , we aim to ascertain whether a critical point exists where the properties of the language, constructed based on the one-dimensional Potts model (the simplest statistical mechanical model), undergo a qualitative and abrupt change. At the critical point of the phase transition, the magnetization, as defined in Eq. (S-3.1), becomes non-differentiable with respect to a control parameter, which is temperature in this paper, in the thermodynamic limit ( $N \rightarrow \infty$ ).

### B. Derivation of Eq. (S-3.3)

The derivation of Eq. (S-3.3) can be shown via the mathematical induction. That is,  $[e_{k+1}]_{k+1}$  is computed as follows:

$$[e_{k+1}]_{k+1} = \sqrt{1 - \sum_{l=1}^k [e_{k+1}]_l^2} \quad (\text{S-3.4})$$

$$= \sqrt{1 - \sum_{l=1}^k \left( -\sqrt{\frac{K}{(K-(l-1))(K-1)(K-l)}} \right)^2} \quad (\text{S-3.5})$$

$$= \sqrt{1 - \sum_{l=1}^k \frac{K}{(K-(l-1))(K-1)(K-l)}} \quad (\text{S-3.6})$$

$$= \sqrt{1 - \frac{K}{K-1} \sum_{l=1}^k \frac{1}{(K-(l-1))(K-l)}} \quad (\text{S-3.7})$$

$$= \sqrt{1 - \frac{K}{K-1} \sum_{l=1}^k \left( \frac{1}{K-l} - \frac{1}{K-(l-1)} \right)} \quad (\text{S-3.8})$$

$$= \sqrt{1 - \frac{K}{K-1} \left( \frac{1}{K-k} - \frac{1}{K} \right)} \quad (\text{S-3.9})$$

$$= \sqrt{1 - \frac{k}{(K-1)(K-k)}} \quad (\text{S-3.10})$$

$$= \sqrt{\frac{K(K-k-1)}{(K-1)(K-k)}}. \quad (\text{S-3.11})$$

Thus, Eq. (S-3.3) holds for  $k+1$ .

### C. Susceptibility

Next, we define the susceptibility as follows:

$$\chi := N(\langle M^2 \rangle - \langle M \rangle^2). \quad (\text{S-3.12})$$

The susceptibility, Eq. (S-3.12), is known to diverge just above the critical point and is well studied due to its ease of experimental measurement, e.g. the  $q$ -state clock model [24, 25]. We also note that the following form is another candidate to define the susceptibility:

$$\tilde{\chi} := N(\langle \mathbf{M} \cdot \mathbf{M} \rangle - \langle \mathbf{M} \rangle \cdot \langle \mathbf{M} \rangle) \quad (\text{S-3.13})$$

$$= N\langle \mathbf{M} \cdot \mathbf{M} \rangle \quad (\text{S-3.14})$$

$$= N\langle M^2 \rangle. \quad (\text{S-3.15})$$

However, Eq. (S-3.15) is known to be valid only for the paramagnetic phase.

### D. Binder parameter

The non-differentiability of the magnetization, as expressed in Eq. (S-3.1), and the divergence of susceptibility, as defined in Eq. (S-3.12), are fundamental characteristics of phase transitions. However, in numerical experiments, encountering challenges in achieving the thermodynamic limit ( $N \rightarrow \infty$ ) due to finite system sizes is common. Consequently, analysis utilizing the Binder parameter is often preferred [26, 27]. The Binder parameter is defined as follows:

$$U := -\frac{K-1}{2} \left( \frac{\langle (\mathbf{M} \cdot \mathbf{M})^2 \rangle}{\langle \mathbf{M} \cdot \mathbf{M} \rangle^2} - \frac{K^2-1}{(K-1)^2} \right) \quad (\text{S-3.16})$$

$$= -\frac{K-1}{2} \left( \frac{\langle M^4 \rangle}{\langle M^2 \rangle^2} - \frac{K+1}{K-1} \right). \quad (\text{S-3.17})$$

It is noteworthy that when  $\mathbf{M}$  is sampled from the Gaussian function with  $K$  degrees of freedom,  $\frac{\langle M^4 \rangle}{\langle M^2 \rangle^2}$  evaluates to  $\frac{K^2-1}{(K-1)^2}$ . Consequently, Eq. (S-3.17) equals 0 for the disordered state and 1 when all the spin variables assume the same value. It is known that at the critical point, the temperature dependence of the Binder parameter, as defined in Eq. (S-3.17), for different system sizes has an intersection. Moreover, it is also recognized to diverge negatively at non-critical phase transition points. Hence, the method of investigating the system size dependence of the Binder parameter, as defined in Eq. (S-3.17), has become standard for identifying phase transition points in numerical computations. From a statistical perspective, the Binder parameter is analogous to kurtosis; it quantifies the tailedness of probability distributions.

### E. Correlation function

By using  $\{\mathbf{e}_k\}_{k=1}^K$  in Eq. (S-3.3), we define the following correlation function:

$$G(i, j) := \langle (\mathbf{e}_{\sigma_i} - \langle \mathbf{e}_{\sigma_i} \rangle) \cdot (\mathbf{e}_{\sigma_j} - \langle \mathbf{e}_{\sigma_j} \rangle) \rangle \quad (\text{S-3.18})$$

$$= \langle \mathbf{e}_{\sigma_i} \cdot \mathbf{e}_{\sigma_j} \rangle - \langle \mathbf{e}_{\sigma_i} \rangle \cdot \langle \mathbf{e}_{\sigma_j} \rangle. \quad (\text{S-3.19})$$

In Eq. (S-3.19), the following quantity is an essential part:

$$\tilde{G}(i, j) := \langle \mathbf{e}_{\sigma_i} \cdot \mathbf{e}_{\sigma_j} \rangle. \quad (\text{S-3.20})$$

Similarly to Eq. (S-3.15), we compute Eq. (S-3.20) instead of Eq. (S-3.19). After some algebra, we get the following correlation function from Eq. (S-3.20) [28]:

$$\tilde{G}(i, j) = \frac{K \langle \delta_{\sigma_i, \sigma_j} \rangle - 1}{K - 1}. \quad (\text{S-3.21})$$

The correlation function is considered to be essential for the research of phase transitions since it decays polynomially at critical points, at which second-order phase transition, and decays exponentially otherwise.

### F. Mutual information

Mutual information also quantifies the correlation between two random variables [29, 30]:

$$I(i, j) = \sum_{\sigma_i, \sigma_j=1}^K p(\sigma_i, \sigma_j) \ln \frac{p(\sigma_i, \sigma_j)}{p(\sigma_i)p(\sigma_j)}. \quad (\text{S-3.22})$$

In Ref. [29], the scaling law of mutual information for CFGs is reported.

### G. Histogram of the magnetization

The histogram of the magnetization, Eq. (S-3.1), is defined as, for  $M$ , letting  $n$  be an integer that satisfies  $M \in [n\Delta M, (n+1)\Delta M)$ ,

$$\text{hist}(M) := \#\{M_i | M_i \in [n\Delta M, (n+1)\Delta M)\}, \quad (\text{S-3.23})$$

where  $M_i$  is the magnetization, Eq. (S-3.1), of the  $i$ -th MC sample for  $i = 1, 2, \dots, N_{\text{MC}}$ . Furthermore,  $N_{\text{MC}}$  is the number of MC samples and  $\Delta M$  is the discretization interval.

In second-order phase transitions, the histogram of the magnetization, as defined in Eq. (S-3.23), transitions from a distribution with a peak at  $M = 0$  for high  $k_{\text{B}}T$  above the critical temperature to a uniform distribution at the critical point. Subsequently, it transitions to a distribution with a peak at  $M = 1$  for low  $k_{\text{B}}T$  below the critical temperature. On the other hand, in first-order phase transitions, the histogram of the magnetization, as defined in Eq. (S-3.23), exhibits two peaks at the transition temperature. This phenomenon is attributed to hysteresis.

### H. Finite-size scaling

In thermodynamics, we are interested in physical quantities in the thermodynamic limit ( $N \rightarrow \infty$ ); however, it is obviously impossible to take this limit in numerical simulations. Finite-size scaling is one of the numerical method based on the scaling assumption to infer the behavior of physical quantities in the thermodynamic limit from numerical results of finite size systems by extrapolate physical quantities of several system sizes.

Let us consider the system size and temperature dependence  $A$ :  $A(L, T)$ . In general, we can consider any parameter instead of temperature  $T$  or even multiple parameters at the same time. At  $T \sim T_c$ ,  $A(L, T)$  is empirically known to behave in the thermodynamic limit as follows:

$$A(L, T) = t^{-x_A}, \quad (\text{S-3.24})$$

where  $x_A$  is the critical exponent of  $A$  and

$$t := \left| \frac{T_c - T}{T_c} \right|. \quad (\text{S-3.25})$$

Similarly, the correlation length  $\xi_\infty$  is divergent as

$$\xi_\infty \propto t^{-\nu}. \quad (\text{S-3.26})$$

where  $\nu$  is the critical exponent of the correlation length. The scaling assumption states that there exists a function  $f_A(\cdot)$  for  $A(L, T)$  such that

$$A(L, T) = L^{\frac{x_A}{\nu}} f_A\left(\frac{L}{\xi_\infty}\right). \quad (\text{S-3.27})$$

Eq. (S-3.24) for  $\tilde{\chi}$ , Eq. (S-3.15), reads

$$\tilde{\chi}(T) \propto t^{-\gamma}, \quad (\text{S-3.28})$$

where  $\gamma$  is the critical exponent for  $\tilde{\chi}$ , Eq. (S-3.15). The scaling assumption, Eq. (S-3.27), for  $\tilde{\chi}$ , Eq. (S-3.15), becomes

$$\frac{\tilde{\chi}(T, L)}{L^{\frac{\gamma}{\nu}}} = f_{\tilde{\chi}}(Lt^{\nu}) \quad (\text{S-3.29})$$

$$= \tilde{f}_{\tilde{\chi}}(L^{\frac{1}{\nu}}t). \quad (\text{S-3.30})$$

Note that  $\tilde{f}_{\tilde{\chi}}(\cdot)$  is also a universal function for  $\tilde{\chi}$ , Eq. (S-3.15). We confirm Eq. (S-3.30) in the main text.

#### S-IV. NUMERICAL SIMULATIONS

We conduct Monte Carlo simulations  $80 \times 80$  times and present the numerical results of the physical quantities defined in Sec. S-III for the proposed model, as described in Eq. (S-2.1). Additionally, considering the rule  $X \rightarrow YZ$  (where symbols are added with equal probability) from Eq. (S-2.1b), we also examine the case  $X \rightarrow XX$  (where symbols are duplicated). In this paper, we investigate the cases of  $K = 2$  and  $K = 10$  setting  $J = 1.0$ .

In this section, we provide all the calculations of physical quantities discussed in Sec. S-III for  $K = 2, 10$  and  $X \rightarrow YZ, XX$ . First of all, we show the magnetization, the susceptibility, and the Binder parameter. Second, we plot the correlation functions and mutual information. Third, we depict the histogram of the magnetization.

Next, we show the system-size dependence of the magnetization, the susceptibilities, and the Binder parameter. We draw the phase diagrams. We see that the phase diagram drastically changes depending on  $X \rightarrow YZ$  and  $X \rightarrow XX$ . We then plot the results of the finite-size scaling method. We see that the critical exponents are independent from the choice of  $X \rightarrow YZ$  or  $X \rightarrow XX$  but varies depending on  $q$ . Finally, we plot the  $q$ -dependence of the critical exponents  $\nu$  and  $\gamma$ .

For  $K = 10$ , we show the relative frequencies of alphabets. In the literature of natural language processing, the relative frequencies of alphabets are known to often satisfy Zipf's law.

##### A. Case where 2 symbols are increasing at random: $K = 2$ and $X \rightarrow YZ$

Let us consider the case where  $K = 2$  and  $X \rightarrow YZ$  (symbols added with equal probability). Since there are two non-terminal symbols and they increase randomly, there are eight processes to consider:

$$\begin{aligned} A &\rightarrow AA, A \rightarrow AB, A \rightarrow BA, A \rightarrow BB, \\ B &\rightarrow AA, B \rightarrow AB, B \rightarrow BA, B \rightarrow BB. \end{aligned} \quad (\text{S-4.1})$$

It is assumed that these processes occur with equal probability for  $A$  and  $B$ .

##### 1. Magnetization, susceptibility, and Binder parameter

In Fig. S-1, the temperature dependence of the magnetization, Eq. (S-3.1), is shown for  $q = 10^{-2.0}, 10^{-0.5}$ . In the case of  $q = 10^{-2.0}$ , as the system size  $N$  increases below the transition point  $T \lesssim 1$ , the magnetization converges to a nonzero value, while above the transition point, it converges to zero. This behavior is consistent with the critical  $\mathbb{Z}_2$  symmetry breaking observed alongside the intersection of the Binder parameters. On the other hand, in the case of  $q = 10^{-0.5}$ ,  $\langle M \rangle$  increases toward  $k_B T = 0$ , but it seems to hover around zero for any temperature. Therefore, Fig. S-1 implies that critical behaviors of the CSG of interest, as described in Eq. (S-2.1), strongly depend on the value of  $q$ .

Next, we show the susceptibility, Eq. (S-3.12), in Fig. S-2. Figure S-2 is consistent with Fig. S-1 since it illustrates a diverging behavior of the susceptibility, typical for a second-order phase transition, at a specific temperature in the case of  $q = 10^{-2.0}$ . Additionally, it monotonically increases toward zero temperature without exhibiting any peaks.

In Fig. S-3, the Binder parameter, Eq. (S-3.17), is shown. In Fig. S-3(left), a clear intersection of the Binder parameter is visible, indicating the presence of a critical point around  $k_B T \sim 1.0$ , while there is no crossing of the Binder parameter in Fig. S-3(right).

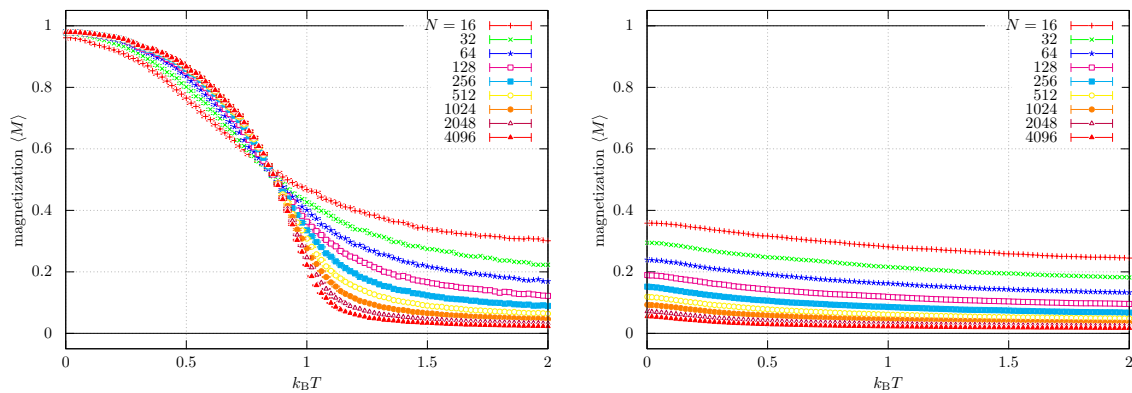


FIG. S-1: Temperature dependence of the magnetization, Eq. (S-3.1), for  $X \rightarrow YZ$ . We set (left)  $q = 10^{-2.0}$  and (right) with  $q = 10^{-0.5}$ . We also set  $K = 2$ ,  $J = 1.0$ ,  $t = 0$ ,  $s = 0.9$ , and  $r_- = r_+ = 0.25$ . The length of the generated sentence by the language model,  $N$ , was varied from 16 to 4096.

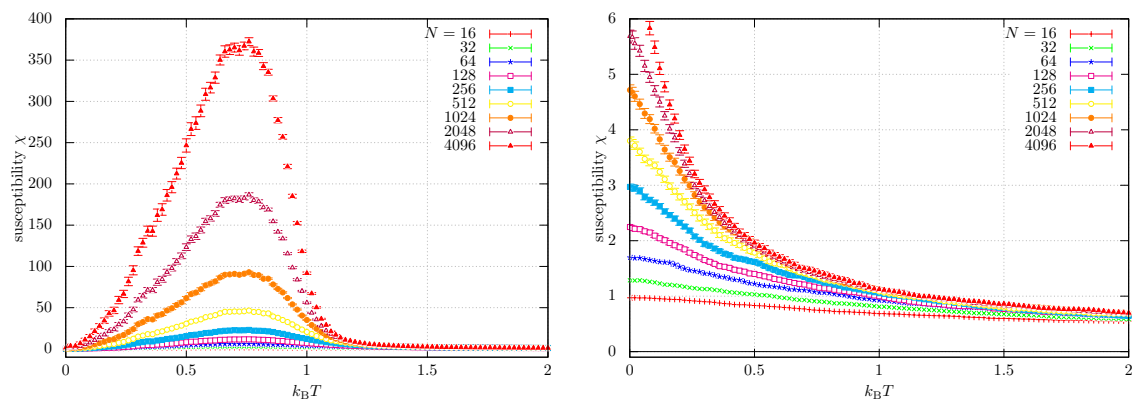


FIG. S-2: Temperature dependence of the susceptibility, Eq. (S-3.12), for  $X \rightarrow YZ$ . We set (left)  $q = 10^{-2.0}$  and (right) with  $q = 10^{-0.5}$ . We also set  $K = 2$ ,  $J = 1.0$ ,  $t = 0$ ,  $s = 0.9$ , and  $r_- = r_+ = 0.25$ . The length of the generated sentence by the language model,  $N$ , was varied from 16 to 4096.

## 2. Correlation functions, mutual information, and histogram of magnetization for $q = 10^{-2.0}$

In Fig. S-4, we display two types of correlation functions. The first one, defined by Eq. (S-3.20) with  $i = 2048$  and  $j = 2048 + \Delta i$ , quantifies the correlation between symbols  $i$  and  $j$  within a given temporal sentence. It is equivalent to the conventional correlation function studied in research on spin systems. The second type, defined by Eq. (S-3.20) with  $i = 0$  and  $j = \lfloor N/4 \rfloor - 1$ , measures how symbols correlate with each other throughout the generation process. This type of correlation function is especially pertinent to models where the length of the generated sentence by the language models,  $N$ , grows and cannot be defined for conventional spin models. Figure S-4(left) illustrates that for high  $k_B T$ , the correlation function decays rapidly with  $\Delta i$ , while for small  $k_B T$ , there is still correlation even for large  $\Delta i$ . Additionally, the correlation function appears to satisfy the scaling behavior around  $k_B T \sim 1.1$ . In Fig. S-4(right), the scaling law seems to hold for  $T \in [0.7, 1.1]$ .

In Fig. S-5, we plot mutual information. Similarly to Fig. S-4(left), the scaling law seems to hold for  $k_B T \sim 1.0$ .

Finally, we show the histogram of the magnetization, Eq. (S-3.23), in Fig. S-6. The histogram of the magnetization, Eq. (S-3.23), in Fig. S-6 is almost uniform at  $k_B T \sim 0.9$ , and this behavior is typical for the second-order phase transition. And for smaller  $k_B T \sim 0.9$ , it has a sharp peak around zero and for larger  $k_B T \sim 0.9$ , it has a sharp peak around 1. Thus, we can numerically conclude that there is a second-order phase transition under the above numerical simulations.

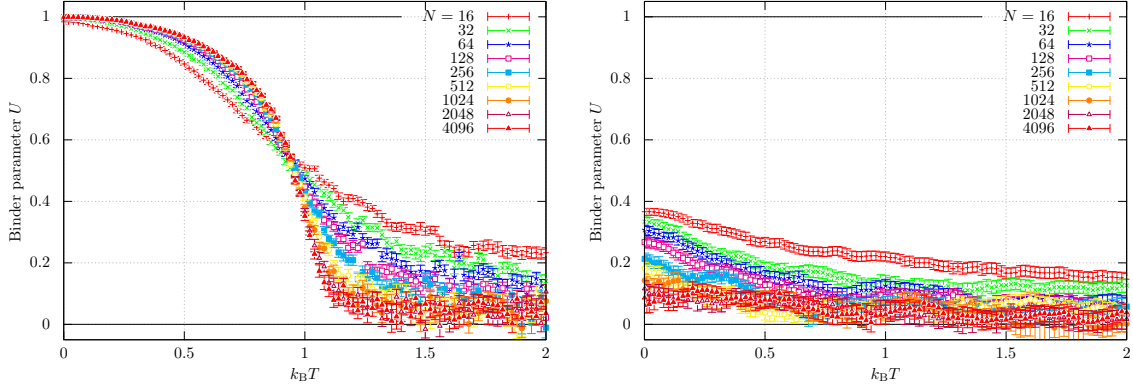


FIG. S-3: Temperature dependence of the Binder parameter, Eq. (S-3.17), for  $X \rightarrow YZ$ . We set (left)  $q = 10^{-2.0}$  and (right) with  $q = 10^{-0.5}$ . We also set  $K = 2$ ,  $J = 1.0$ ,  $t = 0$ ,  $s = 0.9$ , and  $r_- = r_+ = 0.25$ . The length of the generated sentence by the language model,  $N$ , was varied from 16 to 4096.

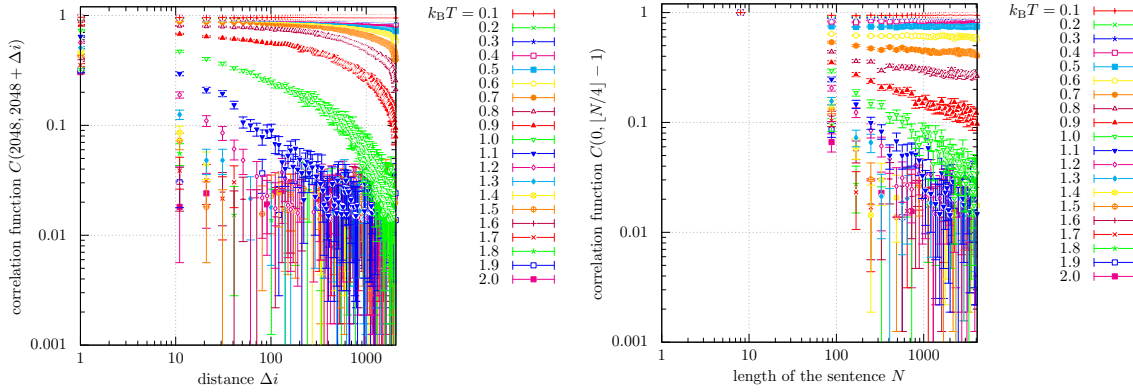


FIG. S-4: Correlation functions, Eq. (S-3.20) (left) with  $i = 2048$  and  $j = 2048 + \Delta i$  and (right) with  $i = 0$  and  $j = \lfloor N/4 \rfloor - 1$  for  $X \rightarrow YZ$ . We set  $K = 2$ ,  $J = 1.0$ ,  $q = 10^{-2.0}$ ,  $t = 0$ ,  $s = 0.9$ , and  $r_- = r_+ = 0.25$ . Temperature  $k_B T$  was varied from 0.1 to 2.0.

### 3. Correlation functions, mutual information, and histogram of magnetization for $q = 10^{-0.5}$

In Fig. S-7, we plot the correlation functions. In Fig. S-8, we show mutual information. In Fig. S-9, the histogram of the magnetization, Eq. (S-3.23), is shown. These figures are all consistent with the fact that the state is in the trivial "paramagnetic" state.

### 4. System-size dependence of the magnetization, the susceptibilities, and the Binder parameter

In Fig. S-10, we show the system-size dependence of the magnetization, Eq. (S-3.1) at  $q = 10^{-2.0}$ .

In Fig. S-11, we plot the system-size dependence the two susceptibilities, Eqs. (S-3.12) and (S-3.15) at  $q = 10^{-2.0}$ . The critical temperature was determined by assessing whether the line was linear or not.

In Fig. S-12, we depict the system-size dependence of the Binder parameter, Eq. (S-3.17), at  $q = 10^{-2.0}$

### 5. Phase diagram, finite-size scaling, and $q$ -dependence of critical exponents

In Fig. S-13, we plot the phase diagram of our language model with  $K = 2$  and  $X \rightarrow YZ$ . We determined the boundary between the two phase by fitting a quadratic function via least square regression. This figure shows that the BKT phase exists for  $k_B T \lesssim 0.20$ .

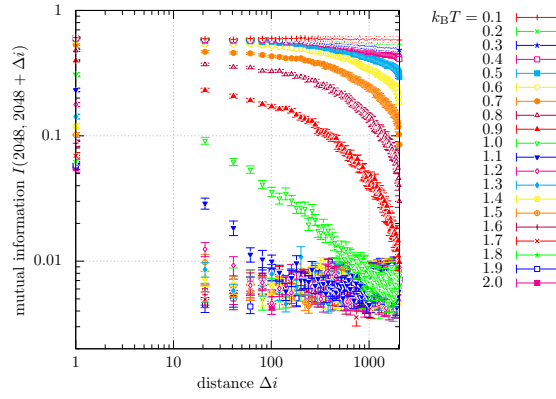


FIG. S-5: Mutual information, Eq. (S-3.22), with  $i = 2048$  and  $j = 2048 + \Delta i$  for  $X \rightarrow YZ$ . We set  $K = 2$ ,  $J = 1.0$ ,  $q = 10^{-2.0}$ ,  $t = 0$ ,  $s = 0.9$ , and  $r_- = r_+ = 0.25$ . Temperature  $k_B T$  was varied from 0.1 to 2.0.

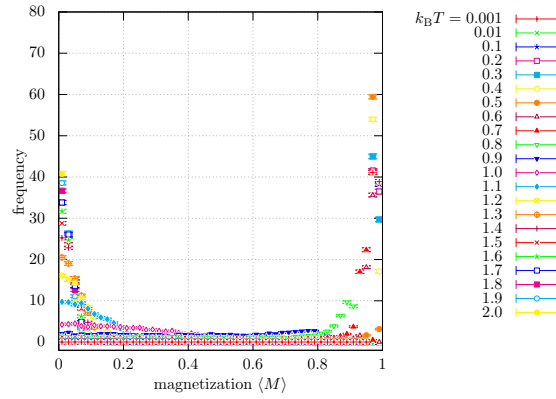


FIG. S-6: Histogram of the magnetization, Eq. (S-3.1), for  $X \rightarrow YZ$ . We set  $K = 2$ ,  $J = 1.0$ ,  $q = 10^{-2.0}$ ,  $t = 0$ ,  $s = 0.9$ , and  $r_- = r_+ = 0.25$ . Temperature  $k_B T$  was varied from 0.1 to 2.0.

In Fig. S-14, we performed finite-size scaling to  $\tilde{\chi}$  at  $q = 10^{-2.0}$ . We set  $T_c = 0.960$ ,  $\nu = 2.50$ , and  $\gamma = 2.05$ , where we have determined the values of  $\nu$  and  $\gamma$  such that the scaling assumption holds; this figure shows that the scaling assumption holds. In Fig. S-15, we set  $T_c = 0.960$ ,  $\nu = 2.29$ , and  $\gamma = 2.05$ , where  $\nu$  and  $\gamma$  are taken from Ref. [14]; the critical exponents are different from the one-dimensional long-range Ising model. More specifically, the critical exponents depend on the value of  $q$ .

In Fig. S-16, we plot the  $q$ -dependence of the critical exponents  $\nu$  and  $\gamma$ .

### B. Case where 2 symbols duplicates: $K = 2$ and $X \rightarrow XX$

We consider the case of  $K = 2$  and  $X \rightarrow XX$  (symbol replication). Since there are two non-terminal symbols, there are two processes:

$$A \rightarrow AA, \quad B \rightarrow BB. \quad (\text{S-4.2})$$

Furthermore, these two processes occur with equal probability. Note that this model can be regarded as a generalization of the Pólya urn model since Eq. (S-2.1) becomes it in the limit of  $t \rightarrow 0$  and  $q \rightarrow 1$ .

#### 1. Magnetization, susceptibility, and Binder parameter

In Fig. S-17, the magnetization, Eq. (S-3.1), for  $q = 10^{-2.0}$  and  $q = 10^{-0.5}$  are shown. For  $q = 10^{-2.0}$ , the behavior of the magnetization, Eq. (S-3.1), is similar to the case of  $X \rightarrow YZ$  shown in Fig. S-1. On the other hand, the

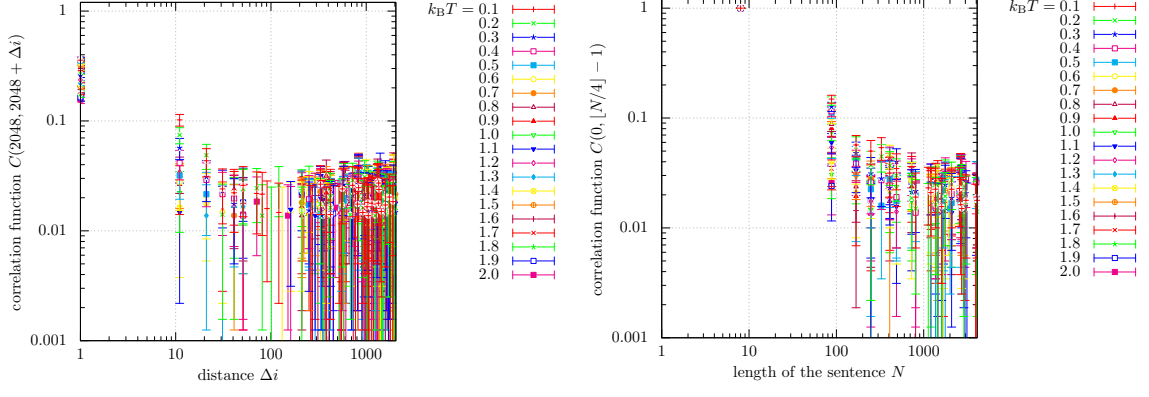


FIG. S-7: Correlation functions, Eq. (S-3.20) (left) with  $i = 2048$  and  $j = 2048 + \Delta i$  and (right) with  $i = 0$  and  $j = \lfloor N/4 \rfloor - 1$  for  $X \rightarrow YZ$ . We set  $K = 2$ ,  $J = 1.0$ ,  $q = 10^{-0.5}$ ,  $t = 0$ ,  $s = 0.9$ , and  $r_- = r_+ = 0.25$ . Temperature  $k_B T$  was varied from 0.1 to 2.0.

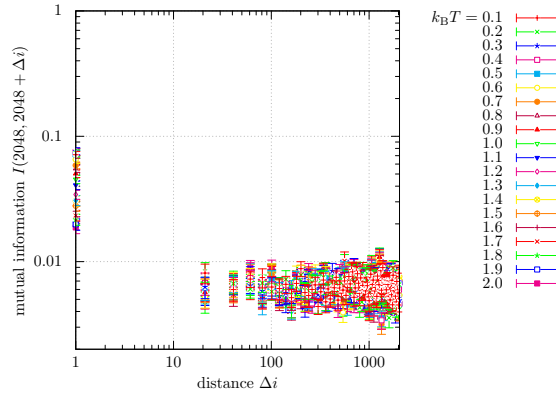


FIG. S-8: Mutual information, Eq. (S-3.22), with  $i = 2048$  and  $j = 2048 + \Delta i$  for  $X \rightarrow YZ$ . We set  $K = 2$ ,  $J = 1.0$ ,  $q = 10^{-0.5}$ ,  $t = 0$ ,  $s = 0.9$ , and  $r_- = r_+ = 0.25$ . Temperature  $k_B T$  was varied from 0.1 to 2.0.

behavior of the magnetization, Eq. (S-3.1), is quite different for  $X \rightarrow XX$  and  $X \rightarrow YZ$ . That is, in Fig. S-17(right), the magnetization seems to have a nontrivial value for small  $k_B T$ .

In Fig. S-18, we show the susceptibility, Eq. (S-3.12). As expected, Fig. S-18 shows diverging behavior for finite temperatures in both cases.

In Fig. S-19, we plot the Binder parameters. In Fig. S-19, we can observe the crossings of the Binder parameters. This fact implies that in the case of  $X \rightarrow XX$  there is a second-order phase transition for a wide range of  $q$ .

## 2. Correlation functions, mutual information, and histogram of magnetization for $q = 10^{-2.0}$

In Fig. S-20, we show the correlation function, Eq. (S-3.20). In Fig. S-21, mutual information, Eq. (S-3.22), is plotted. In Fig. S-22, we plot the histogram of the magnetization, Eq. (S-3.23). These figures are consistent with the second-order phase transition.

## 3. Correlation functions, mutual information, and histogram of magnetization for $q = 10^{-0.5}$

In Fig. S-23, we show the correlation function, Eq. (S-3.20). In Fig. S-24, we plot the histogram of the magnetization, Eq. (S-3.23). In Fig. S-25, we plot the histogram of the magnetization, Eq. (S-3.23). These figures are also consistent with the second-order phase transition.

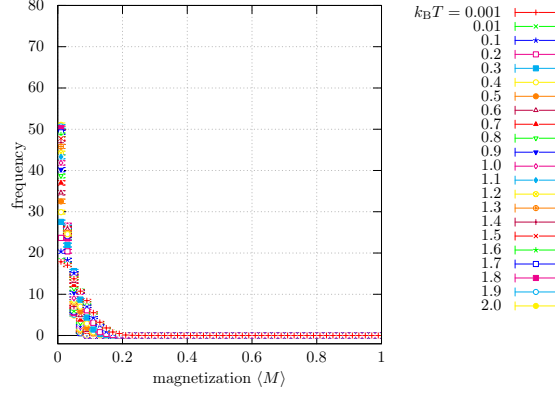


FIG. S-9: Histogram of the magnetization, Eq. (S-3.1), for  $X \rightarrow YZ$ . We set  $K = 2$ ,  $J = 1.0$ ,  $q = 10^{-0.5}$ ,  $t = 0$ ,  $s = 0.9$ , and  $r_- = r_+ = 0.25$ . Temperature  $k_B T$  was varied from 0.1 to 2.0.

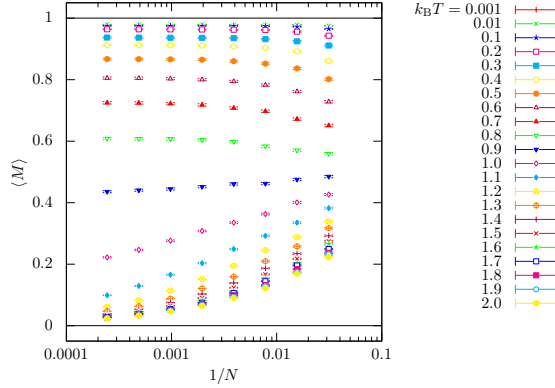


FIG. S-10: System-size dependence of the magnetization, Eq. (S-3.1), at  $q = 10^{-2.0}$ . We consider  $X \rightarrow YZ$  and set  $K = 2$ ,  $J = 1.0$ ,  $t = 0$ ,  $s = 0.9$ , and  $r_- = r_+ = 0.25$ . We varied  $N = 32, 64, 128, 256, 512, 1024, 2048, 4096$ .

#### 4. System-size dependence of the magnetization, the susceptibilities, and the Binder parameter

In Fig. S-26, we show the system-size dependence of the magnetization, Eq. (S-3.1) at  $q = 10^{-2.0}$ .

In Fig. S-27, we plot the system-size dependence the two susceptibilities, Eqs. (S-3.12) and (S-3.15) at  $q = 10^{-2.0}$ . The critical temperature was determined by assessing whether the line was linear or not.

In Fig. S-28, we depict the system-size dependence of the Binder parameter, Eq. (S-3.17), at  $q = 10^{-2.0}$

#### 5. Phase diagram, finite-size scaling, and $q$ -dependence of critical exponents

In Fig. S-29, we plot the phase diagram of our language model with  $K = 2$  and  $X \rightarrow XX$ . We determined the boundary between the two phase by fitting a quadratic function via least square regression. In the case of  $X \rightarrow XX$ , the regime of the BKT phase is drastically expanded especially for large  $q$  compared with the case of  $X \rightarrow YZ$ .

In Fig. S-30, we performed finite-size scaling to  $\tilde{\chi}$  at  $q = 10^{-2.0}$ . We set  $T_c = 1.0$ ,  $\nu = 2.50$  and  $\gamma = 2.05$ , where we have determined the values of  $\nu$  and  $\gamma$  such that the scaling assumption holds. This figure states that the scaling assumption holds. In Fig. S-31, we set  $T_c = 1.0$ ,  $\nu = 2.29$ , and  $\gamma = 2.05$ , where  $\nu$  and  $\gamma$  are taken from Ref. [14]. Similarly to the case of  $X \rightarrow YZ$ , the critical exponents depend on the value of  $q$ .

In Fig. S-32, we plot the  $q$ -dependence of the critical exponents  $\nu$  and  $\gamma$ .

### C. Case where 10 symbols are increasing at random: $K = 10$ and $X \rightarrow YZ$

Here we consider the case where 10 symbols increase at random.

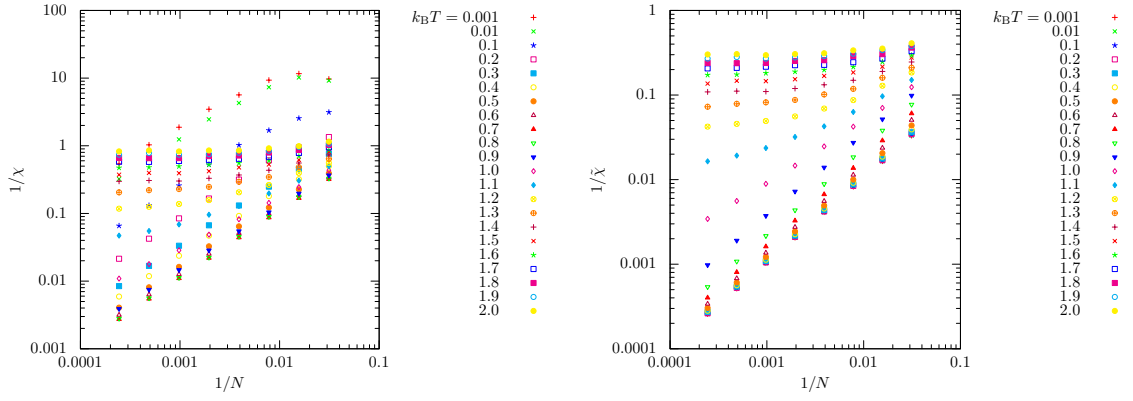


FIG. S-11: System-size dependence of the susceptibilities, (left) Eq. (S-3.12) and (right) Eq. (S-3.15) at  $q = 10^{-2.0}$ . We consider  $X \rightarrow YZ$  and set  $K = 2$ ,  $J = 1.0$ ,  $t = 0$ ,  $s = 0.9$ , and  $r_- = r_+ = 0.25$ . We varied  $N = 32, 64, 128, 256, 512, 1024, 2048, 4096$ .

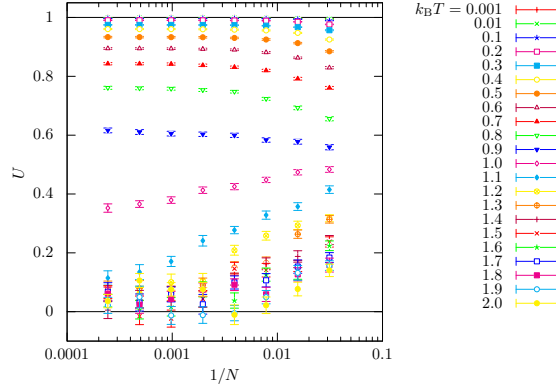


FIG. S-12: System-size dependence of the Binder parameter, Eq. (S-3.17), at  $q = 10^{-2.0}$ . We consider  $X \rightarrow YZ$  and set  $K = 2$ ,  $J = 1.0$ ,  $t = 0$ ,  $s = 0.9$ , and  $r_- = r_+ = 0.25$ . We varied  $N = 32, 64, 128, 256, 512, 1024, 2048, 4096$ .

### 1. Magnetization, susceptibility, and Binder parameter

In Fig. S-33, we plot the magnetization, Eq. (S-3.1). Figure S-33 shows that the magnetization grows for small  $k_B T$  in the case of  $q = 10^{-2.0}$ , but it remains in a trivial state for both  $q = 10^{-2.0}$  and  $q = 10^{-0.5}$ .

In Fig. S-34, we show the susceptibility, Eq. (S-3.12). This figure is consistent with Figure S-33 because there is no peak for finite temperature while the susceptibility grows or even looks diverging for  $q = 10^{-2.0}$ .

In Fig. S-35, we show the Binder parameter. As expected, the Binder parameter does not go to 1 for small  $k_B T$ . But we can see the dip for  $q = 10^{-2.0}$ . This fact implies that there is a first-order phase transition at  $T \rightarrow 0$ .

### 2. Correlation functions, mutual information, and histogram of magnetization for $q = 10^{-2.0}$

In Fig. S-36, we show the correlation functions, Eq. (S-3.20). The behavior of the correlation function with  $i = 2048$  and  $j = 2048 + \Delta i$  shown in Fig. S-36(left) look similar to that of the first-order phase transition since it changed from concave functions to convex functions lowering temperature without becoming a straight line in the log-log plot. On the other hand, the correlation function with  $i = 0$  and  $j = \lfloor N/4 \rfloor - 1$  shown in Fig. S-36(right) shows straight lines in the log-log plot for a wide range of  $k_B T$ .

In Fig. S-37, the histogram of the magnetization, Eq. (S-3.23), is shown. The novel point of Fig. S-37 is that the histogram has two peaks toward  $k_B T = 0$ , and this implies that there is a first-order phase transition at  $k_B T = 0$ .

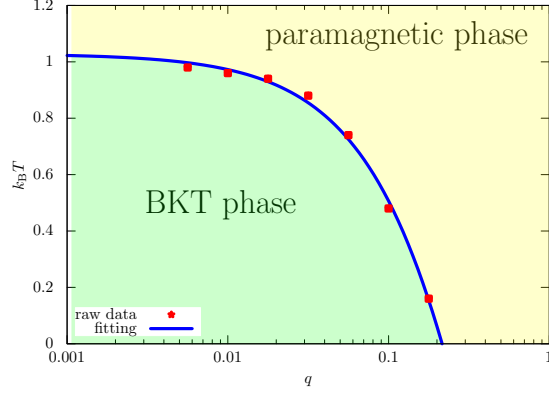


FIG. S-13: Phase diagram of the CSG model investigated in this paper where the horizontal and vertical axes are the growth rate of a sentence  $q$  and temperature  $k_B T$ , respectively. We consider  $X \rightarrow YZ$  and set  $K = 2$ ,  $J = 1.0$ ,  $t = 0$ ,  $s = 0.9$ , and  $r_- = r_+ = 0.25$ .

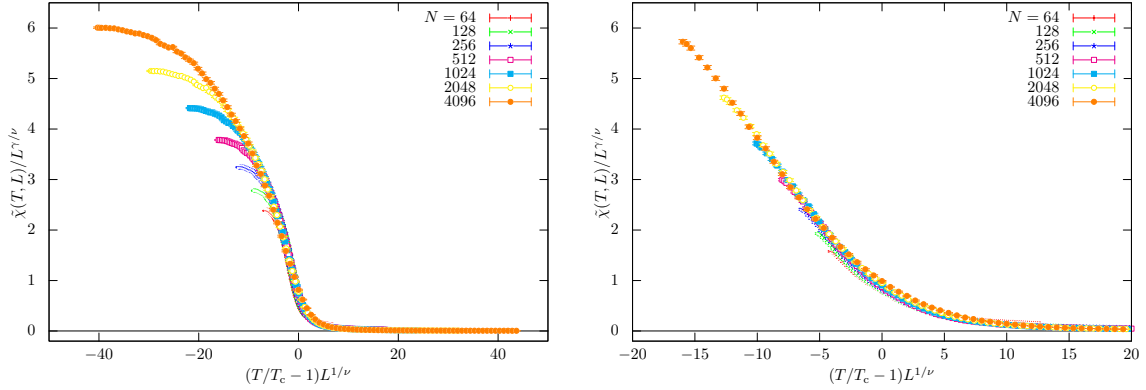


FIG. S-14: Finite-size scaling of  $\tilde{\chi}$  at (left)  $q = 10^{-2.0}$  and (right)  $q = 10^{-1.0}$ . We set  $T_c = 0.960$ ,  $\nu = 2.50$ , and  $\gamma = 2.05$  for  $q = 10^{-2.0}$  and  $T_c = 0.48$ ,  $\nu = 3.0$ , and  $\gamma = 2.05$  for  $q = 10^{-1.0}$ , where the values of  $\nu$  and  $\gamma$  are determined such that the scaling assumption holds. We consider  $X \rightarrow YZ$  and set  $K = 2$ ,  $J = 1.0$ ,  $t = 0$ ,  $s = 0.9$ , and  $r_- = r_+ = 0.25$ . We varied  $N = 64, 128, 256, 512, 1024, 2048, 4096$ .

### 3. Correlation functions, mutual information, and histogram of magnetization for $q = 10^{-0.5}$

In Fig. S-38, the correlation function, Eq. (S-3.20), is shown. In Fig. S-39, we show the histogram of the magnetization, Eq. (S-3.23). The above figures consistently implies that the state is always in the trivial state without any singularities.

### 4. System-size dependence of the magnetization, the susceptibilities, and the Binder parameter

In Fig. S-40, we show the system-size dependence of the magnetization, Eq. (S-3.1) at  $q = 10^{-2.0}$ .

In Fig. S-41, we plot the system-size dependence the two susceptibilities, Eqs. (S-3.12) and (S-3.15) at  $q = 10^{-2.0}$ . The critical temperature was determined by assessing whether the line was linear or not.

In Fig. S-42, we depict the system-size dependence of the Binder parameter, Eq. (S-3.17), at  $q = 10^{-2.0}$

### 5. Phase diagram, finite-size scaling, and $q$ -dependence of critical exponents

In Fig. S-43, we plot the phase diagram of our language model with  $K = 10$  and  $X \rightarrow YZ$ . We determined the boundary between the two phase by fitting a quadratic function via least square regression. Compared to the case of  $K = 2$ , the regime of the BKT phase is shrunk.

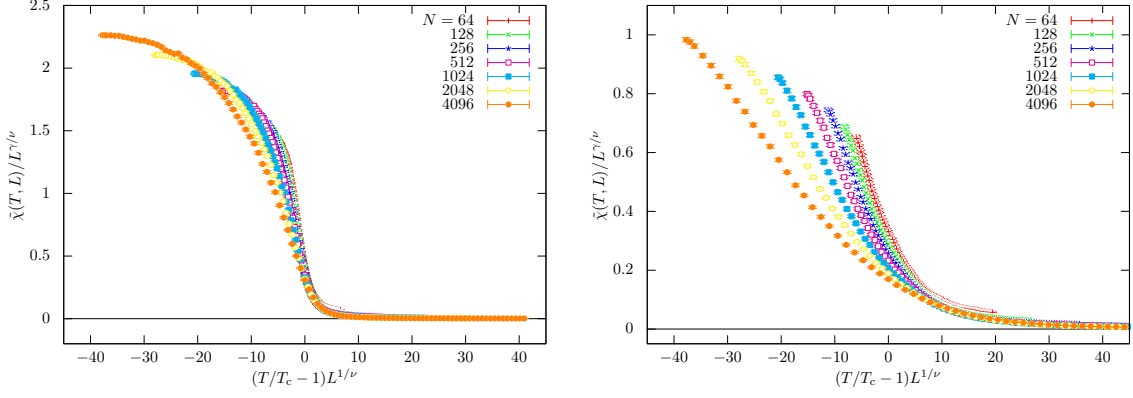


FIG. S-15: Finite-size scaling of  $\tilde{\chi}$  at (left)  $q = 10^{-2.0}$  and (right)  $q = 10^{-1.0}$ . We set  $T_c = 0.960$  for  $q = 10^{-2.0}$  and  $T_c = 0.48$  for  $q = 10^{-1.0}$ . We also set  $\nu = 2.29$ , and  $\gamma = 2.05$ , where the values of  $\nu$  and  $\gamma$  are taken from Ref. [14]. We consider  $X \rightarrow YZ$  and set  $K = 2$ ,  $J = 1.0$ ,  $t = 0$ ,  $s = 0.9$ , and  $r_- = r_+ = 0.25$ . We varied  $N = 64, 128, 256, 512, 1024, 2048, 4096$ .

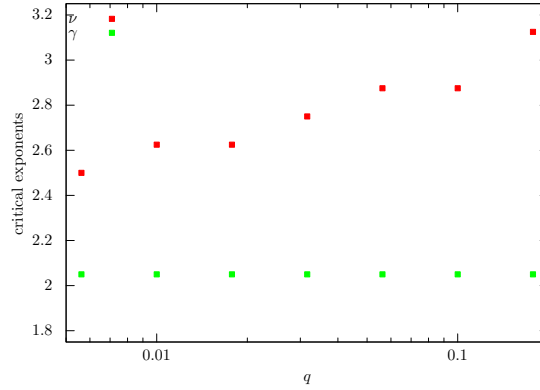


FIG. S-16:  $q$ -dependence of the critical exponents  $\nu$  and  $\gamma$ . We consider  $X \rightarrow YZ$  and set  $K = 2$ ,  $J = 1.0$ ,  $t = 0$ ,  $s = 0.9$ , and  $r_- = r_+ = 0.25$ .

In Fig. S-44, we performed finite-size scaling to  $\tilde{\chi}$  at  $q = 10^{-2.0}$ . We set  $T_c = 0.40$ ,  $\nu = 2.0$ , and  $\gamma = 1.25$ , where  $\nu$  and  $\gamma$  are determined such that the scaling assumption holds.

In Fig. S-45, we plot the  $q$ -dependence of the critical exponents  $\nu$  and  $\gamma$ .

### 6. Configurations and relative frequencies for $q = 10^{-2.0}$

As shown in Fig. S-37, the histogram of magnetization has peaks at  $\langle M \rangle = 0.550, 0.790$ . Then, in Fig. S-46, we show typical configurations of which magnetization is 0.550 and 0.790. In both cases, symbols are scattered, but their distributions have a different feature. Around  $\langle M \rangle = 0.790$ , one symbol dominates; on the other hand, near  $\langle M \rangle = 0.550$ , two major symbols are comparatively dominant.

In Fig. S-47, we plot the relative frequencies of alphabets. Symbols on the horizontal axis are sorted by their frequencies. In natural languages, relative frequencies of alphabets often show Zipf's law, that is, they become a straight line in the log-log plot. The relative frequencies at  $k_B T = 0.3000$  seem to be a straight line in Fig. S-47(left). On the other hand, the histogram of alphabets are almost uniformly random at  $k_B T = 0.1000$ , as shown in Fig. S-47(right). In Fig. S-48, we also plot the relative frequencies of alphabets at  $k_B T = 0.0010$ . For alphabets whose relative frequencies are small, we can see Zipf's law.

### D. Case where 10 symbols duplicates: $K = 10$ and $X \rightarrow XX$

Here we consider the case where 10 symbols duplicate.

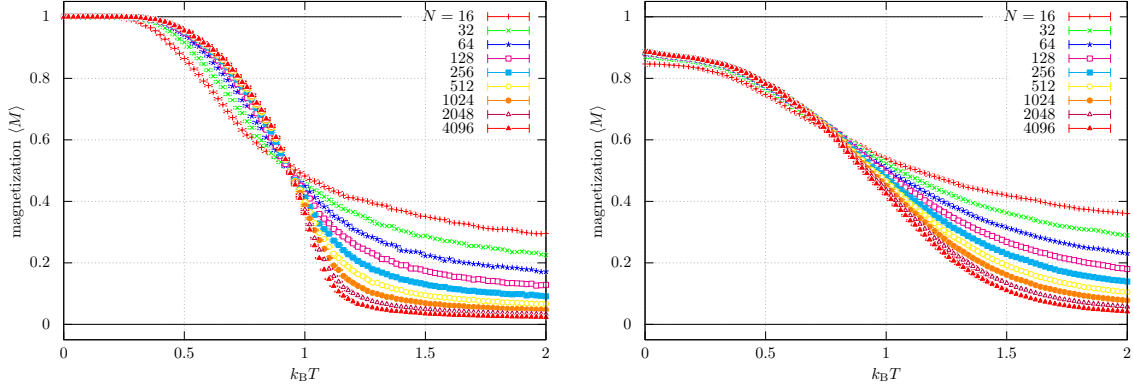


FIG. S-17: Temperature dependence of the magnetization, Eq. (S-3.1), for  $X \rightarrow XX$ . We set (left)  $q = 10^{-2.0}$  and (right) with  $q = 10^{-0.5}$ . We also set  $K = 2$ ,  $J = 1.0$ ,  $q = 10^{-0.5}$ ,  $t = 0$ ,  $s = 0.9$ , and  $r_- = r_+ = 0.25$ . The length of the generated sentence by the language model,  $N$ , was varied from 16 to 4096.

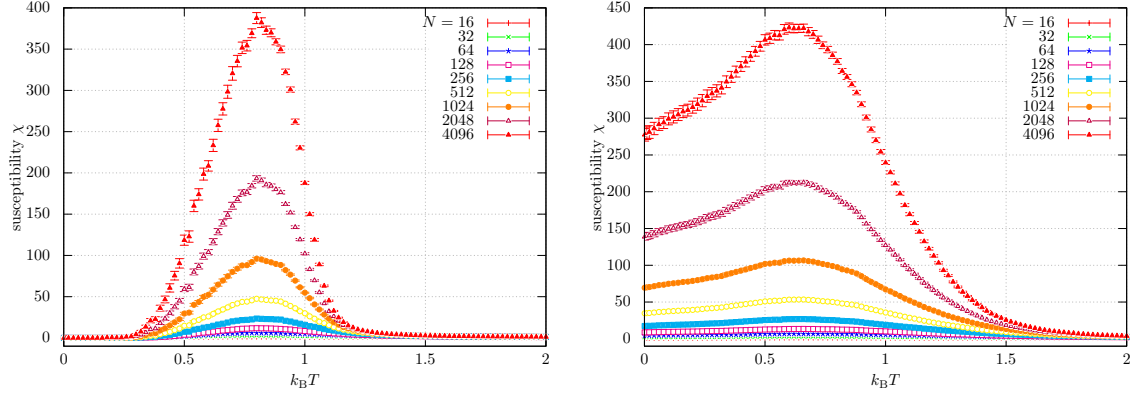


FIG. S-18: Temperature dependence of the susceptibility, Eq. (S-3.12), for  $X \rightarrow XX$ . We set (left)  $q = 10^{-2.0}$  and (right) with  $q = 10^{-0.5}$ . We also set  $K = 2$ ,  $J = 1.0$ ,  $q = 10^{-0.5}$ ,  $t = 0$ ,  $s = 0.9$ , and  $r_- = r_+ = 0.25$ . The length of the generated sentence by the language model,  $N$ , was varied from 16 to 4096.

### 1. Magnetization, susceptibility, and Binder parameter

In Fig. S-49, we plot the magnetization, Eq. (S-3.1). In both cases, the magnetization, Eq. (S-3.1), goes to a nontrivial value when  $k_B T$  is decreased. The magnetization seems to jump near  $k_B T \sim 0.7$  for  $q = 10^{-2.0}$  while it gradually goes up for  $q = 10^{-0.5}$ .

In Fig. S-50, the susceptibility, Eq. (S-3.12) is plotted. In Fig. S-50, the susceptibility has a peak for a specific temperature. This fact also supports the existence of phase transitions.

In Fig. S-51, the Binder parameter, Eq. (S-3.17), is shown. For  $q = 10^{-2.0}$ , the Binder parameter exhibits a sharp dip before reaching 1 as  $k_B T$  decreases. This behavior is characteristic of a first-order phase transition. Similarly, for  $q = 10^{-0.5}$ , the Binder parameter displays a similar trend, albeit without the width of the dip. In both cases, the existence of a first-order phase transition appears evident. However, the exact cause of the wide dip in the Binder parameter is not clear.

### 2. Correlation functions, mutual information, and histogram of magnetization for $q = 10^{-2.0}$

In Fig. S-52, the correlation function, Eq. (S-3.20), is shown. In Fig. S-52(left), the correlation functions transition from concave functions to convex functions as  $k_B T$  decreases. This observation supports the existence of a first-order phase transition. On the other hand, Fig. S-52(right) displays straight lines over a wide range of  $k_B T$ .

In Fig. S-53, we plot the histogram of the magnetization, Eq. (S-3.23). At  $k_B T \sim 0.4$ , there are two peaks. This fact strongly supports the existence of the first-order phase transition.

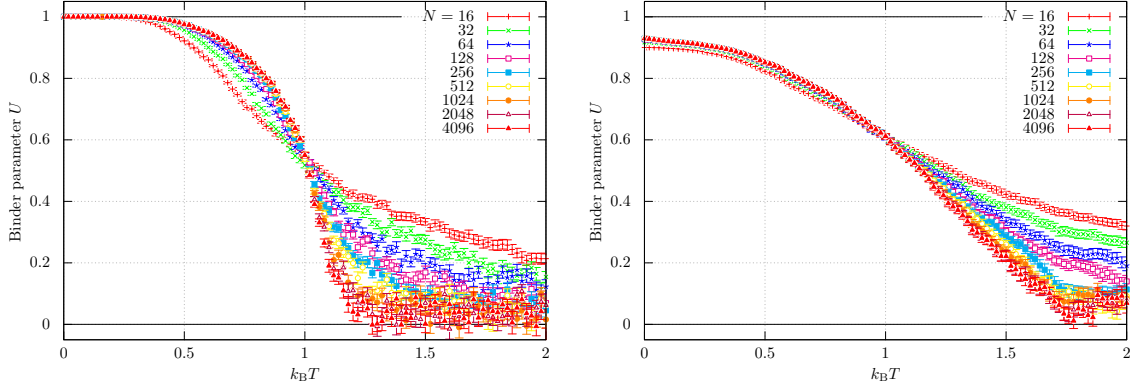


FIG. S-19: Temperature dependence of the Binder parameter, Eq. (S-3.17), for  $X \rightarrow XX$ . We set (left)  $q = 10^{-2.0}$  and (right) with  $q = 10^{-0.5}$ . We also set  $K = 2$ ,  $J = 1.0$ ,  $q = 10^{-0.5}$ ,  $t = 0$ ,  $s = 0.9$ , and  $r_- = r_+ = 0.25$ . The length of the generated sentence by the language model,  $N$ , was varied from 16 to 4096.

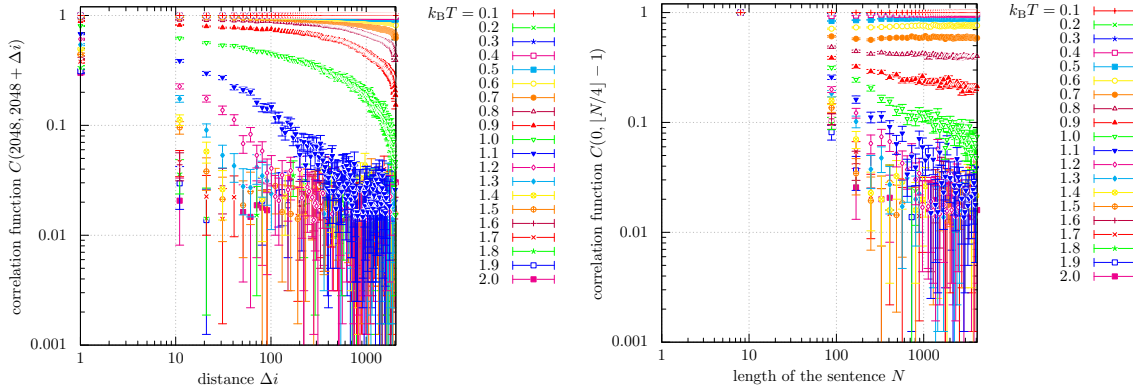


FIG. S-20: Correlation functions, Eq. (S-3.20) (left) with  $i = 2048$  and  $j = 2048 + \Delta i$  and (right) with  $i = 0$  and  $j = \lfloor N/4 \rfloor - 1$  for  $X \rightarrow XX$ . We set  $K = 2$ ,  $J = 1.0$ ,  $q = 10^{-2.0}$ ,  $t = 0$ ,  $s = 0.9$ , and  $r_- = r_+ = 0.25$ . Temperature  $k_B T$  was varied from 0.1 to 2.0.

### 3. Correlation functions, mutual information, and histogram of magnetization for $q = 10^{-0.5}$

In Fig. S-54, the correlation functions are shown. For  $q = 10^{-0.5}$ , the correlation function varies similarly to that of the second-order phase transition.

In Fig. S-55, the histogram of the magnetization, Eq. (S-3.23), is shown. Figure S-55 shows two peaks toward  $k_B T = 0$ . This fact implies that the first-order phase transition occurs at  $k_B T = 0$ .

### 4. System-size dependence of the magnetization, the susceptibilities, and the Binder parameter

In Fig. S-56, we show the system-size dependence of the magnetization, Eq. (S-3.1) at  $q = 10^{-2.0}$ .

In Fig. S-57, we plot the system-size dependence the two susceptibilities, Eqs. (S-3.12) and (S-3.15) at  $q = 10^{-2.0}$ . The critical temperature was determined by assessing whether the line was linear or not.

In Fig. S-58, we depict the system-size dependence of the Binder parameter, Eq. (S-3.17), at  $q = 10^{-2.0}$

### 5. Phase diagram, finite-size scaling, and $q$ -dependence of critical exponents

In Fig. S-59, we plot the phase diagram of our language model with  $K = 10$  and  $X \rightarrow XX$ . We determined the boundary between the two phase by fitting a quadratic function via least square regression.

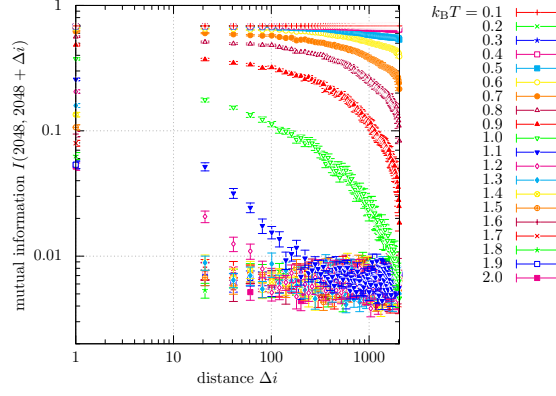


FIG. S-21: Mutual information, Eq. (S-3.22), with  $i = 2048$  and  $j = 2048 + \Delta i$  for  $X \rightarrow XX$ . We set  $K = 2$ ,  $J = 1.0$ ,  $q = 10^{-2.0}$ ,  $t = 0$ ,  $s = 0.9$ , and  $r_- = r_+ = 0.25$ . Temperature  $k_B T$  was varied from 0.1 to 2.0.

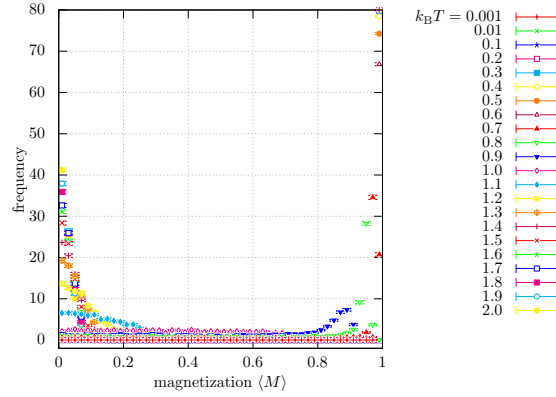


FIG. S-22: Histogram of the magnetization, Eq. (S-3.1), for  $X \rightarrow XX$ . We set  $K = 2$ ,  $J = 1.0$ ,  $q = 10^{-2.0}$ ,  $t = 0$ ,  $s = 0.9$ , and  $r_- = r_+ = 0.25$ . Temperature  $k_B T$  was varied from 0.1 to 2.0.

In Fig. S-60, we performed finite-size scaling to  $\tilde{\chi}$  at  $q = 10^{-2.0}$ . We set  $T_c = 0.640$ ,  $\nu = 2.0$ , and  $\gamma = 1.25$ , where  $\nu$  and  $\gamma$  are such that the scaling assumption holds.

In Fig. S-61, we plot the  $q$ -dependence of the critical exponents  $\nu$  and  $\gamma$ .

### 6. Configurations and relative frequencies for $q = 10^{-2.0}$

In Fig. S-62, we plot typical configurations of which magnetization is 0.670 at  $k_B T = 0.440$  and those of which magnetization is 0.990 at  $k_B T = 0.0010$ . The reason why we set  $k_B T = 0.440$  for configurations of which magnetization is 0.670 is that the histogram has a peak at  $\langle M \rangle = 0.670$  when  $k_B T = 0.440$ . When the magnetization is around 0.670, two symbols are dominant and two states coexist. As expected, the system is ordered when the magnetization is near 0.990.

In Fig. S-63, relative frequencies of alphabets are shown. When the magnetization is around 0.670, two major symbols are dominant and other symbols rarely appear in sentences; as a result, the relative frequencies do not fit Zipf's law. In the case where the magnetization is near 0.990, only a single symbol appears in a sentence.

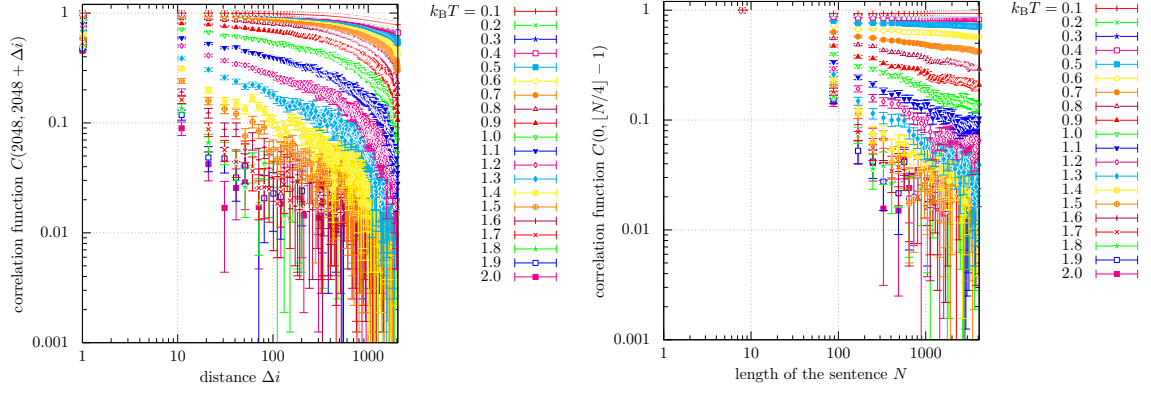


FIG. S-23: Correlation functions, Eq. (S-3.20) (left) with  $i = 2048$  and  $j = 2048 + \Delta i$  and (right) with  $i = 0$  and  $j = \lfloor N/4 \rfloor - 1$  for  $X \rightarrow XX$ . We set  $K = 2$ ,  $J = 1.0$ ,  $q = 10^{-0.5}$ ,  $t = 0$ ,  $s = 0.9$ , and  $r_- = r_+ = 0.25$ . Temperature  $k_B T$  was varied from 0.1 to 2.0.

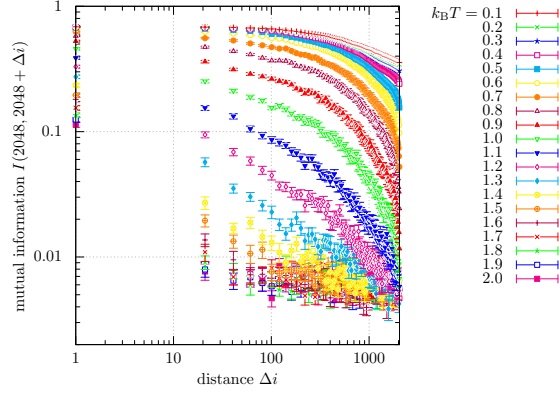


FIG. S-24: Mutual information, Eq. (S-3.22), with  $i = 2048$  and  $j = 2048 + \Delta i$  for  $X \rightarrow XX$ . We set  $K = 2$ ,  $J = 1.0$ ,  $q = 10^{-0.5}$ ,  $t = 0$ ,  $s = 0.9$ , and  $r_- = r_+ = 0.25$ . Temperature  $k_B T$  was varied from 0.1 to 2.0.

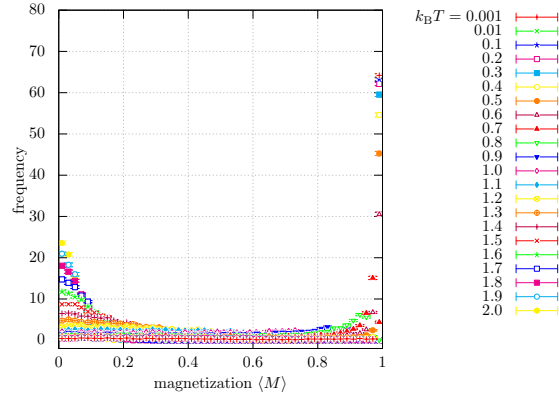


FIG. S-25: Histogram of the magnetization, Eq. (S-3.1), for  $X \rightarrow XX$ . We set  $K = 2$ ,  $J = 1.0$ ,  $q = 10^{-0.5}$ ,  $t = 0$ ,  $s = 0.9$ , and  $r_- = r_+ = 0.25$ . Temperature  $k_B T$  was varied from 0.1 to 2.0.

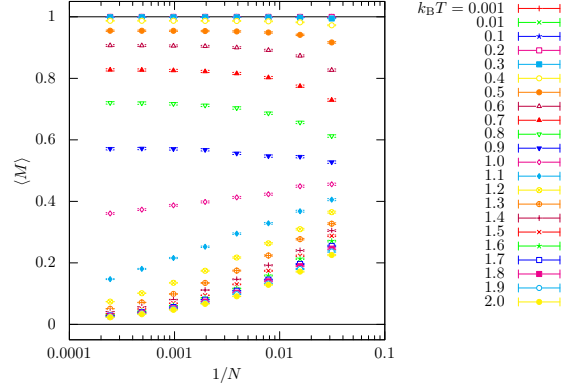


FIG. S-26: System-size dependence of the magnetization, Eq. (S-3.1), at  $q = 10^{-2.0}$ . We consider  $X \rightarrow XX$  and set  $K = 2$ ,  $J = 1.0$ ,  $t = 0$ ,  $s = 0.9$ , and  $r_- = r_+ = 0.25$ . We varied  $N = 32, 64, 128, 256, 512, 1024, 2048, 4096$ .

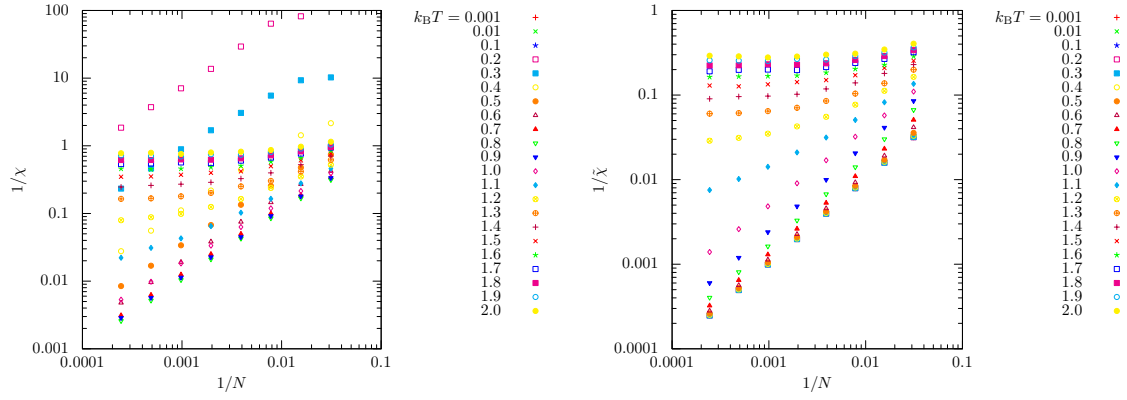


FIG. S-27: System-size dependence of the susceptibilities, (left) Eq. (S-3.12) and (right) Eq. (S-3.15) at  $q = 10^{-2.0}$ . We consider  $X \rightarrow XX$  and set  $K = 2$ ,  $J = 1.0$ ,  $t = 0$ ,  $s = 0.9$ , and  $r_- = r_+ = 0.25$ . We varied  $N = 32, 64, 128, 256, 512, 1024, 2048, 4096$ .

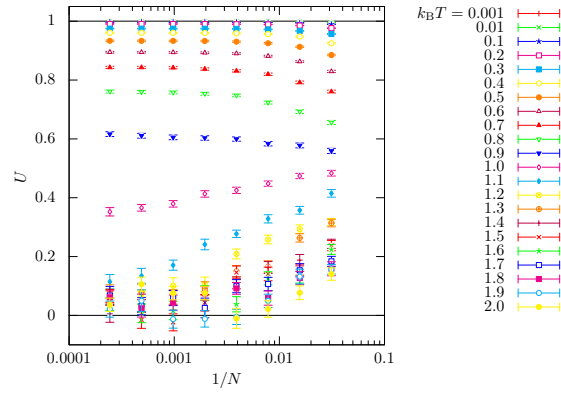


FIG. S-28: System-size dependence of the Binder parameter, Eq. (S-3.17), at  $q = 10^{-2.0}$ . We consider  $X \rightarrow XX$  and set  $K = 2$ ,  $J = 1.0$ ,  $t = 0$ ,  $s = 0.9$ , and  $r_- = r_+ = 0.25$ . We varied  $N = 32, 64, 128, 256, 512, 1024, 2048, 4096$ .

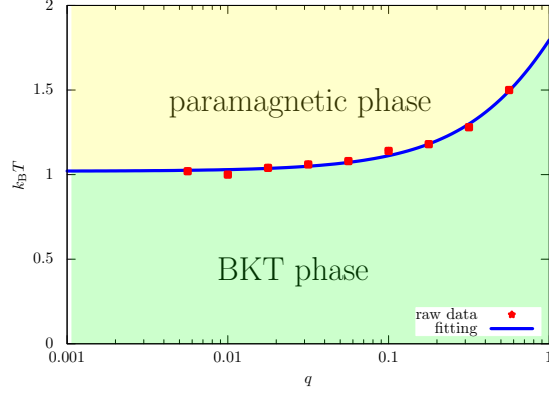


FIG. S-29: Phase diagram of the CSG model investigated in this paper where the horizontal and vertical axes are the growth rate of a sentence  $q$  and temperature  $k_B T$ , respectively. We consider  $X \rightarrow XX$  and set  $K = 2$ ,  $J = 1.0$ ,  $t = 0$ ,  $s = 0.9$ , and  $r_- = r_+ = 0.25$ .

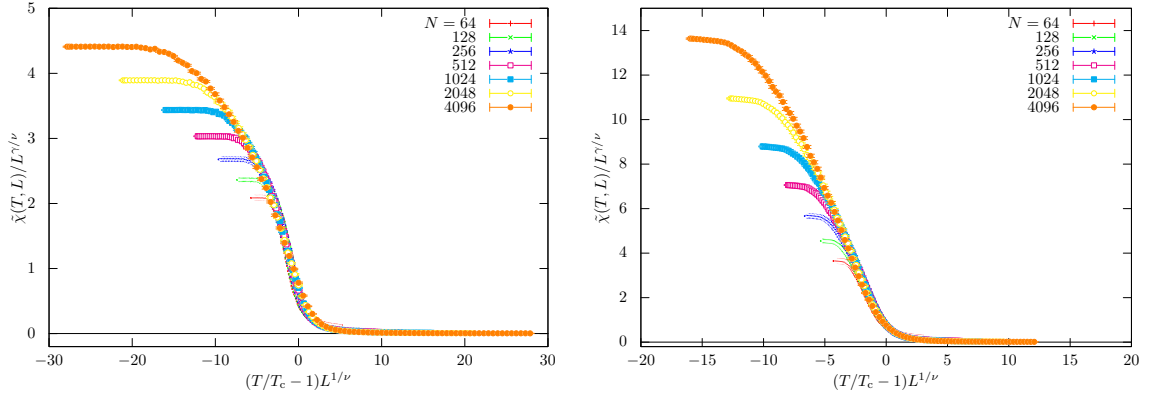


FIG. S-30: Finite-size scaling of  $\tilde{\chi}$  at (left)  $q = 10^{-2.0}$  and (right)  $q = 10^{-1.0}$ . We set  $T_c = 1.0$ ,  $\nu = 2.50$ , and  $\gamma = 2.05$  for  $q = 10^{-2.0}$  and  $T_c = 1.14$ ,  $\nu = 3.0$ , and  $\gamma = 2.05$  for  $q = 10^{-1.0}$ , where the values of  $\nu$  and  $\gamma$  are determined such that the scaling assumption holds. We consider  $X \rightarrow XX$  and set  $K = 2$ ,  $J = 1.0$ ,  $t = 0$ ,  $s = 0.9$ , and  $r_- = r_+ = 0.25$ . We varied  $N = 64, 128, 256, 512, 1024, 2048, 4096$ .

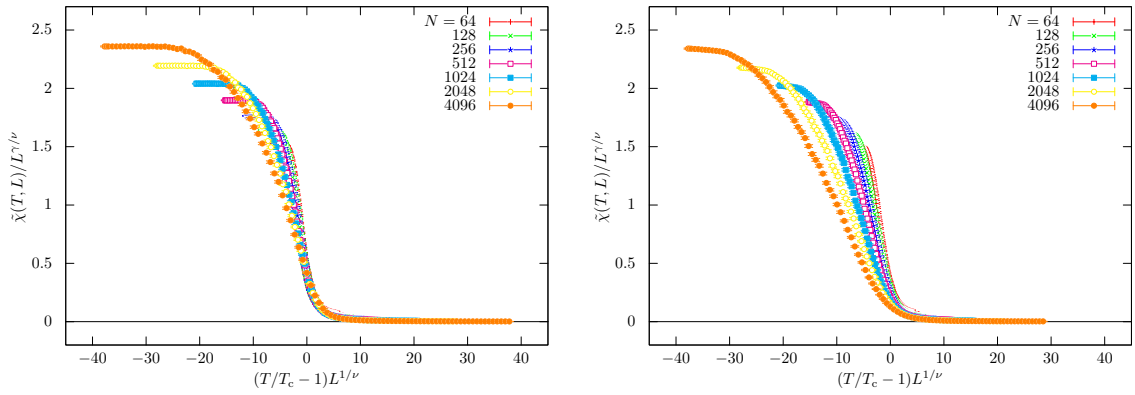


FIG. S-31: Finite-size scaling of  $\tilde{\chi}$  at (left)  $q = 10^{-2.0}$  and (right)  $q = 10^{-1.0}$ . We set  $T_c = 1.0$  for  $q = 10^{-2.0}$  and  $T_c = 1.14$  for  $q = 10^{-1.0}$ . We also set  $\nu = 2.29$ , and  $\gamma = 2.05$ , where the values of  $\nu$  and  $\gamma$  are taken from Ref. [14]. We consider  $X \rightarrow XX$  and set  $K = 2$ ,  $J = 1.0$ ,  $t = 0$ ,  $s = 0.9$ , and  $r_- = r_+ = 0.25$ . We varied  $N = 64, 128, 256, 512, 1024, 2048, 4096$ .

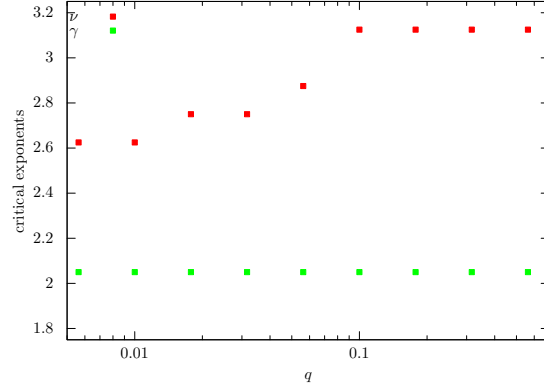


FIG. S-32:  $q$ -dependence of the critical exponents  $\nu$  and  $\gamma$ . We consider  $X \rightarrow XX$  and set  $K = 2$ ,  $J = 1.0$ ,  $t = 0$ ,  $s = 0.9$ , and  $r_- = r_+ = 0.25$ .

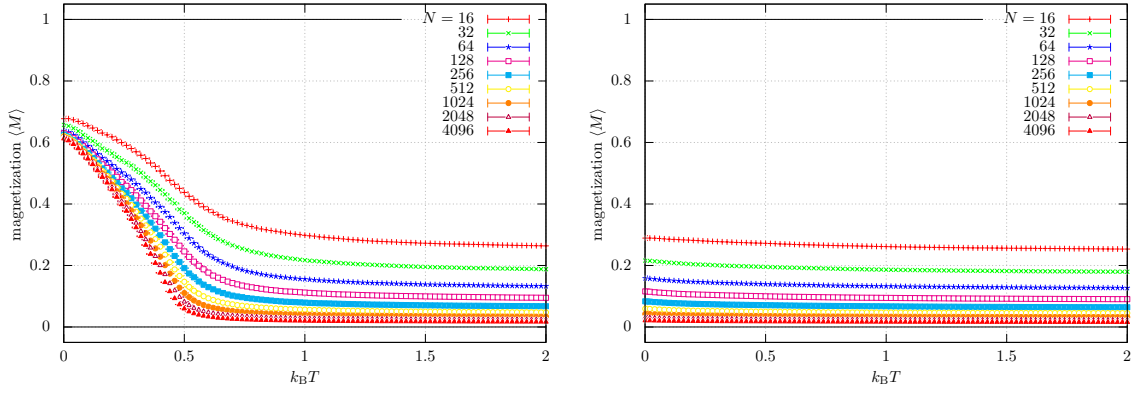


FIG. S-33: Temperature dependence of the magnetization, Eq. (S-3.1), for  $X \rightarrow YZ$ . We set (left)  $q = 10^{-2.0}$  and (right) with  $q = 10^{-0.5}$ . We also set  $K = 10$ ,  $J = 1.0$ ,  $t = 0$ ,  $s = 0.9$ , and  $r_- = r_+ = 0.25$ . The length of the generated sentence by the language model,  $N$ , was varied from 16 to 4096.

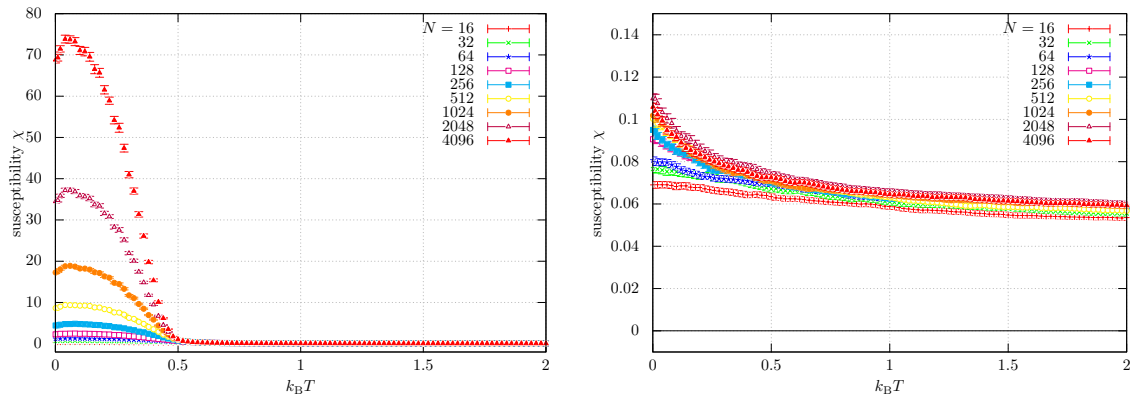


FIG. S-34: Temperature dependence of the susceptibility, Eq. (S-3.12), for  $X \rightarrow YZ$ . We set (left)  $q = 10^{-2.0}$  and (right) with  $q = 10^{-0.5}$ . We also set  $K = 10$ ,  $J = 1.0$ ,  $t = 0$ ,  $s = 0.9$ , and  $r_- = r_+ = 0.25$ . The length of the generated sentence by the language model,  $N$ , was varied from 16 to 4096.

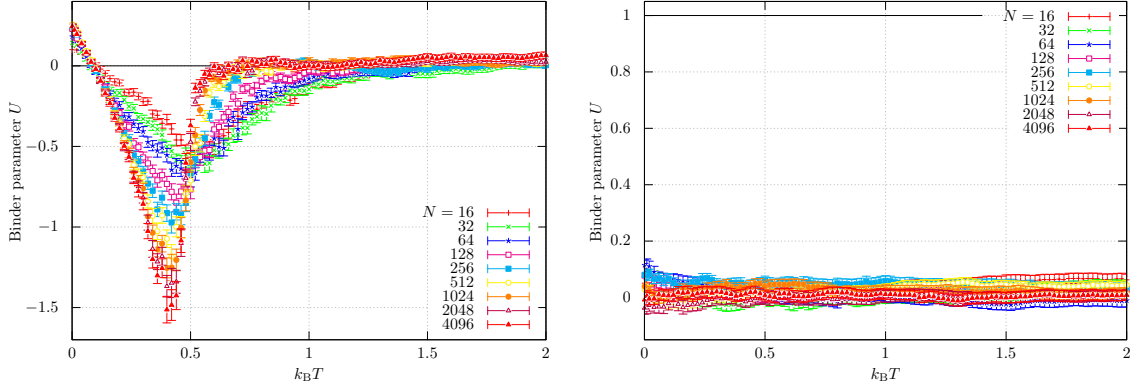


FIG. S-35: Temperature dependence of the Binder parameter, Eq. (S-3.17), for  $X \rightarrow YZ$ . We set (left)  $q = 10^{-2.0}$  and (right) with  $q = 10^{-0.5}$ . We also set  $K = 10$ ,  $J = 1.0$ ,  $t = 0$ ,  $s = 0.9$ , and  $r_- = r_+ = 0.25$ . The length of the generated sentence by the language model,  $N$ , was varied from 16 to 4096.

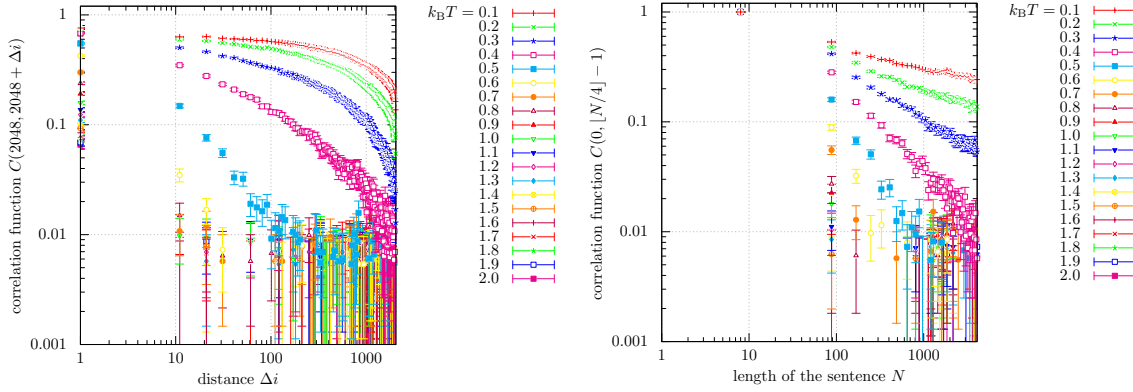


FIG. S-36: Correlation functions, Eq. (S-3.20) (left) with  $i = 2048$  and  $j = 2048 + \Delta i$  and (right) with  $i = 0$  and  $j = \lfloor N/4 \rfloor - 1$  for  $X \rightarrow YZ$ . We set  $K = 10$ ,  $J = 1.0$ ,  $q = 10^{-2.0}$ ,  $t = 0$ ,  $s = 0.9$ , and  $r_- = r_+ = 0.25$ . Temperature  $k_B T$  was varied from 0.1 to 2.0.

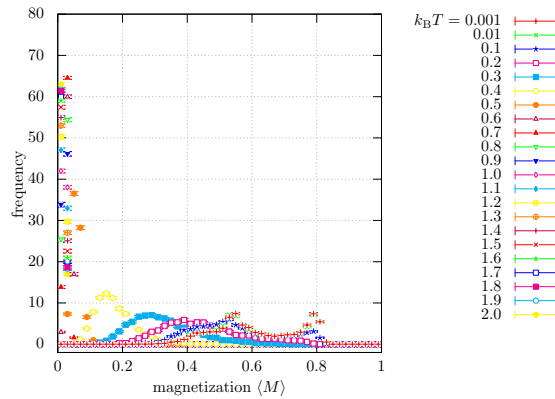


FIG. S-37: Histogram of the magnetization, Eq. (S-3.1), for  $X \rightarrow YZ$ . We set  $K = 10$ ,  $J = 1.0$ ,  $q = 10^{-2.0}$ ,  $t = 0$ ,  $s = 0.9$ , and  $r_- = r_+ = 0.25$ . Temperature  $k_B T$  was varied from 0.1 to 2.0.

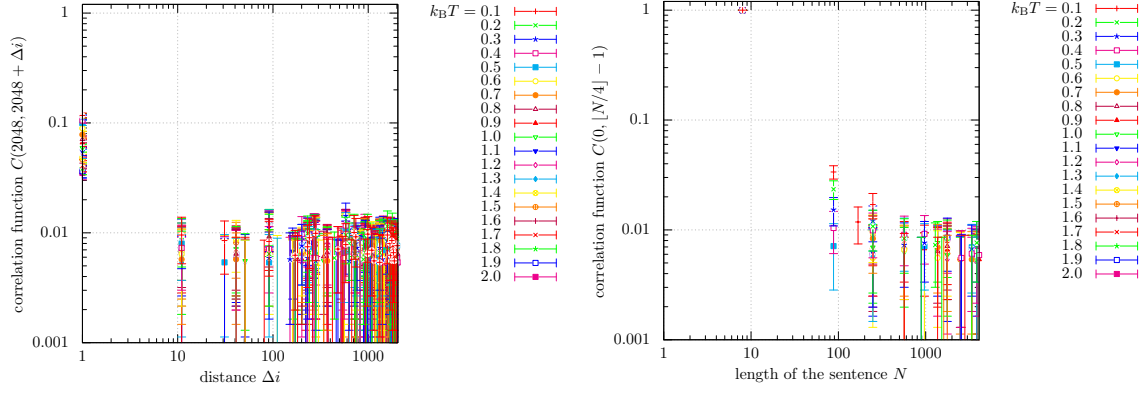


FIG. S-38: Correlation functions, Eq. (S-3.20) (left) with  $i = 2048$  and  $j = 2048 + \Delta i$  and (right) with  $i = 0$  and  $j = \lfloor N/4 \rfloor - 1$  for  $X \rightarrow YZ$ . We set  $K = 10$ ,  $J = 1.0$ ,  $q = 10^{-0.5}$ ,  $t = 0$ ,  $s = 0.9$ , and  $r_- = r_+ = 0.25$ . Temperature  $k_B T$  was varied from 0.1 to 2.0.

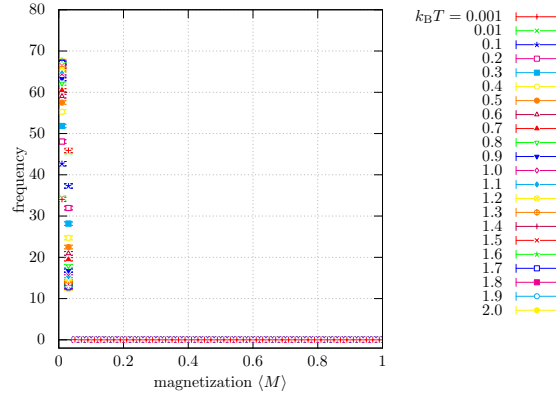


FIG. S-39: Histogram of the magnetization, Eq. (S-3.1), for  $X \rightarrow YZ$ . We set  $K = 10$ ,  $J = 1.0$ ,  $q = 10^{-0.5}$ ,  $t = 0$ ,  $s = 0.9$ , and  $r_- = r_+ = 0.25$ . Temperature  $k_B T$  was varied from 0.1 to 2.0.

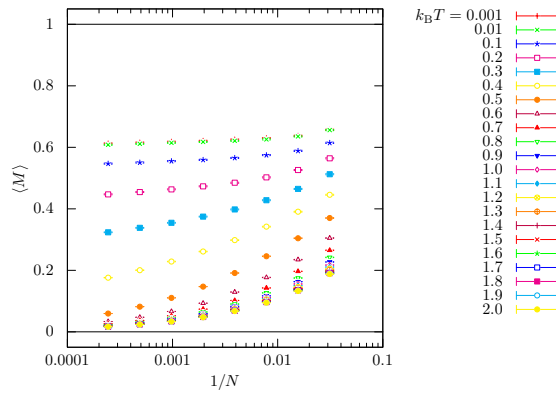


FIG. S-40: System-size dependence of the magnetization, Eq. (S-3.1), at  $q = 10^{-2.0}$ . We consider  $X \rightarrow YZ$  and set  $K = 10$ ,  $J = 1.0$ ,  $t = 0$ ,  $s = 0.9$ , and  $r_- = r_+ = 0.25$ . We varied  $N = 32, 64, 128, 256, 512, 1024, 2048, 4096$ .

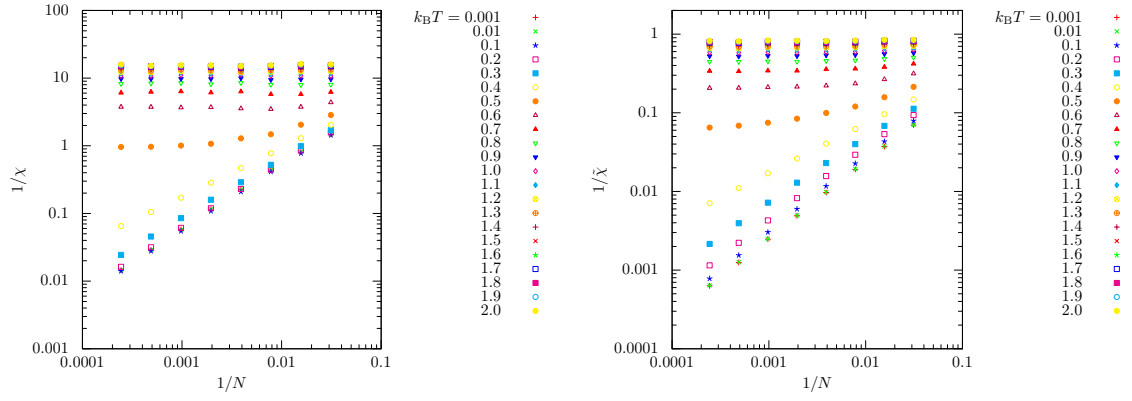


FIG. S-41: System-size dependence of the susceptibilities, (left) Eq. (S-3.12) and (right) Eq. (S-3.15) at  $q = 10^{-2.0}$ . We consider  $X \rightarrow YZ$  and set  $K = 10$ ,  $J = 1.0$ ,  $t = 0$ ,  $s = 0.9$ , and  $r_- = r_+ = 0.25$ . We varied  $N = 32, 64, 128, 256, 512, 1024, 2048, 4096$ .

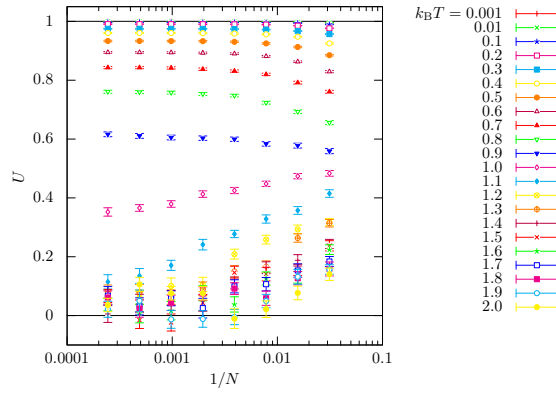


FIG. S-42: System-size dependence of the Binder parameter, Eq. (S-3.17), at  $q = 10^{-2.0}$ . We consider  $X \rightarrow YZ$  and set  $K = 10$ ,  $J = 1.0$ ,  $t = 0$ ,  $s = 0.9$ , and  $r_- = r_+ = 0.25$ . We varied  $N = 32, 64, 128, 256, 512, 1024, 2048, 4096$ .

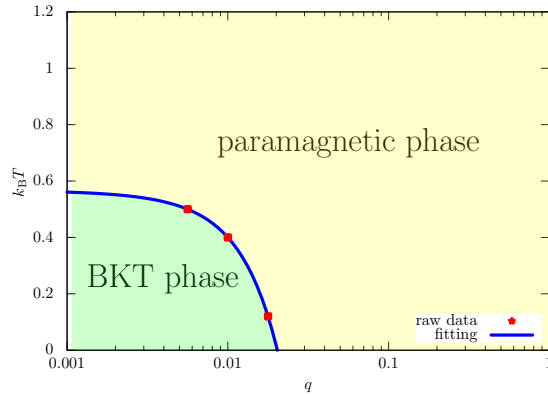


FIG. S-43: Phase diagram of the CSG model investigated in this paper where the horizontal and vertical axes are the growth rate of a sentence  $q$  and temperature  $k_B T$ , respectively. We consider  $X \rightarrow YZ$  and set  $K = 10$ ,  $J = 1.0$ ,  $t = 0$ ,  $s = 0.9$ , and  $r_- = r_+ = 0.25$ .

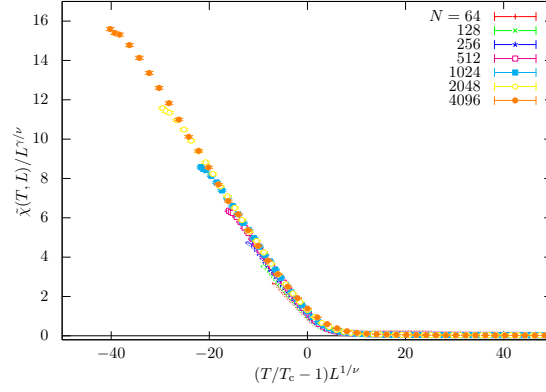


FIG. S-44: Finite-size scaling of  $\tilde{\chi}$  at  $q = 10^{-2.0}$ . We set  $T_c = 0.40$ ,  $\nu = 2.0$ , and  $\gamma = 1.25$ , where the values of  $\nu$  and  $\gamma$  are determined such that the scaling assumption is satisfied. We consider  $X \rightarrow YZ$  and set  $K = 10$ ,  $J = 1.0$ ,  $t = 0$ ,  $s = 0.9$ , and  $r_- = r_+ = 0.25$ . We varied  $N = 64, 128, 256, 512, 1024, 2048, 4096$ .

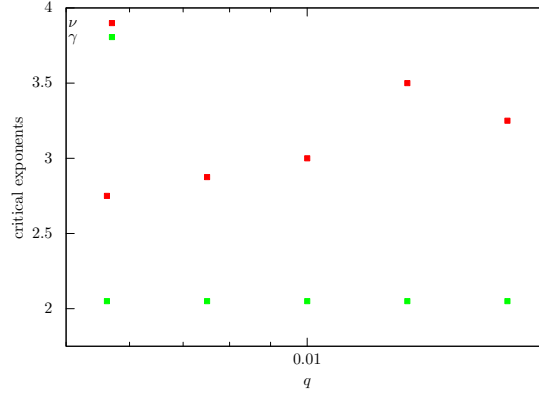


FIG. S-45:  $q$ -dependence of the critical exponents  $\nu$  and  $\gamma$ . We consider  $X \rightarrow YZ$  and set  $K = 10$ ,  $J = 1.0$ ,  $t = 0$ ,  $s = 0.9$ , and  $r_- = r_+ = 0.25$ .

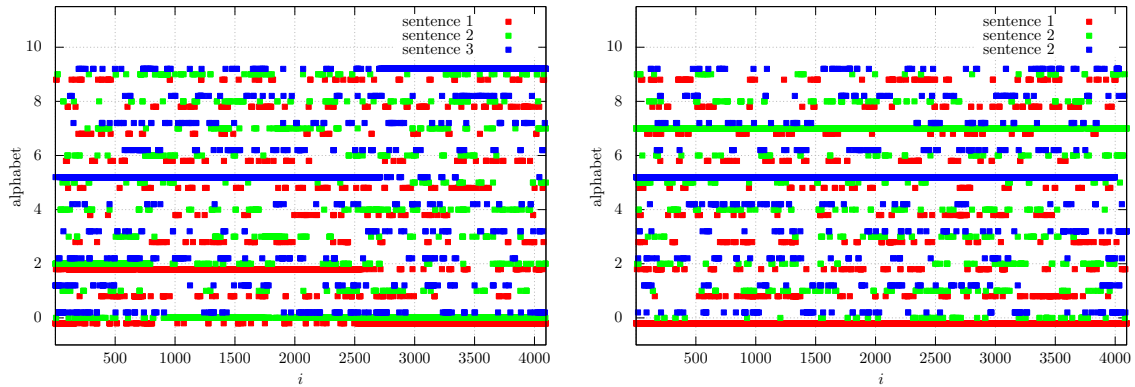


FIG. S-46: Typical configurations of symbols for  $X \rightarrow YZ$ . (left) We considered states of which magnetization lies between 0.5400 and 0.5600 at  $k_B T = 0.0010$ , and (right) states of which magnetization lies between 0.7800 and 0.8000 at  $k_B T = 0.0010$ . We set  $K = 10$ ,  $J = 1.0$ ,  $q = 10^{-2.0}$ ,  $t = 0$ ,  $s = 0.9$ , and  $r_- = r_+ = 0.25$ .

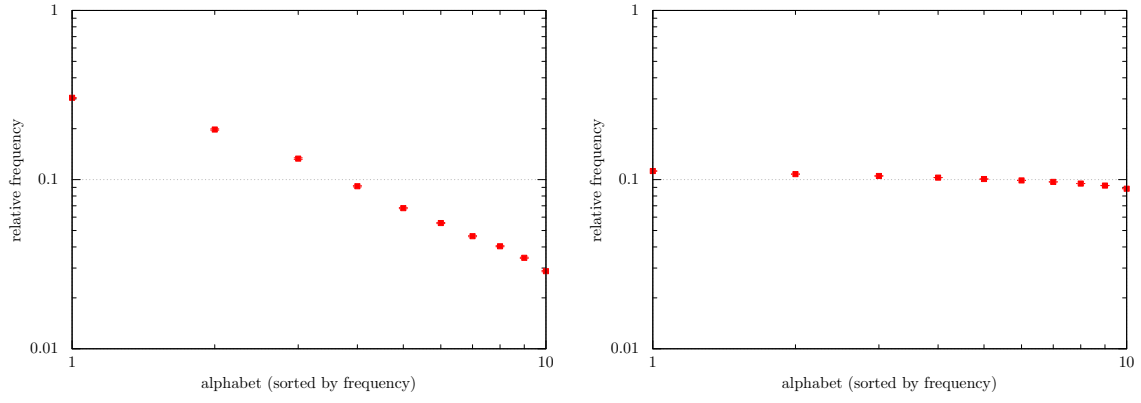


FIG. S-47: Relative frequencies of alphabets for  $X \rightarrow YZ$ . (left) We considered states of which magnetization lies between 0.2800 and 0.3000 at  $k_B T = 0.3000$ , and (right) states of which magnetization lies between 0.0200 and 0.0400 at  $k_B T = 0.1000$ . We set  $K = 10$ ,  $J = 1.0$ ,  $q = 10^{-2.0}$ ,  $t = 0$ ,  $s = 0.9$ , and  $r_- = r_+ = 0.25$ . Symbols on the horizontal axis are sorted by frequencies. The scales of the vertical and horizontal axes are logarithmic.

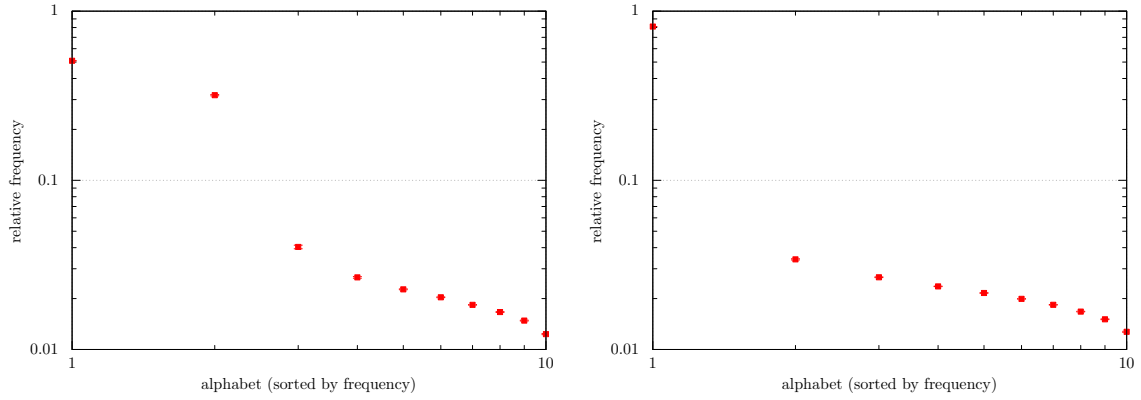


FIG. S-48: Relative frequencies of alphabets for  $X \rightarrow YZ$ . (left) We considered states of which magnetization lies between 0.5400 and 0.5600 at  $k_B T = 0.0010$ , and (right) states of which magnetization lies between 0.7800 and 0.8000 at  $k_B T = 0.0010$ . We set  $K = 10$ ,  $J = 1.0$ ,  $q = 10^{-2.0}$ ,  $t = 0$ ,  $s = 0.9$ , and  $r_- = r_+ = 0.25$ . Symbols on the horizontal axis are sorted by frequencies. The scales of the vertical and horizontal axes are logarithmic.

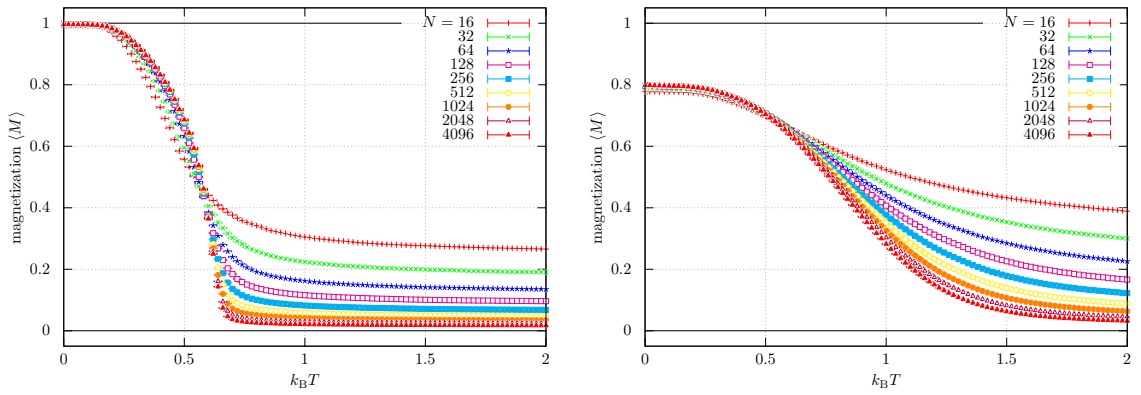


FIG. S-49: Temperature dependence of the magnetization, Eq. (S-3.1), for  $X \rightarrow XX$ . We set (left)  $q = 10^{-2.0}$  and (right) with  $q = 10^{-0.5}$ . We also set  $K = 10$ ,  $J = 1.0$ ,  $q = 10^{-0.5}$ ,  $t = 0$ ,  $s = 0.9$ , and  $r_- = r_+ = 0.25$ . The length of the generated sentence by the language model,  $N$ , was varied from 16 to 4096.

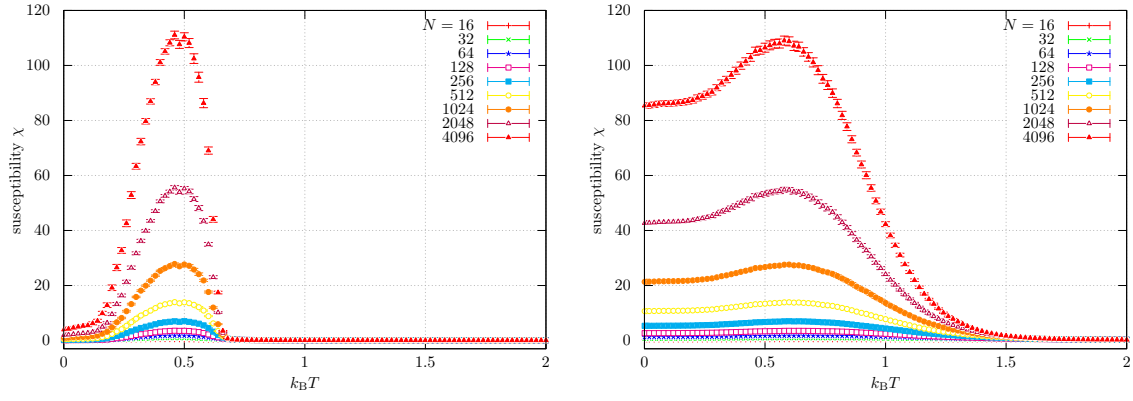


FIG. S-50: Temperature dependence of the susceptibility, Eq. (S-3.12), for  $X \rightarrow XX$ . We set (left)  $q = 10^{-2.0}$  and (right) with  $q = 10^{-0.5}$ . We also set  $K = 10$ ,  $J = 1.0$ ,  $q = 10^{-0.5}$ ,  $t = 0$ ,  $s = 0.9$ , and  $r_- = r_+ = 0.25$ . The length of the generated sentence by the language model,  $N$ , was varied from 16 to 4096.

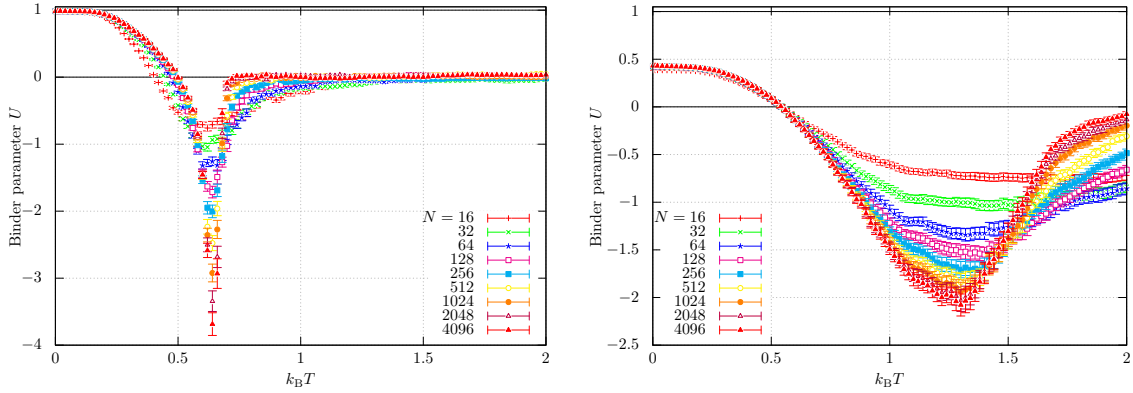


FIG. S-51: Temperature dependence of the Binder parameter, Eq. (S-3.17), for  $X \rightarrow XX$ . We set (left)  $q = 10^{-2.0}$  and (right) with  $q = 10^{-0.5}$ . We also set  $K = 10$ ,  $J = 1.0$ ,  $q = 10^{-0.5}$ ,  $t = 0$ ,  $s = 0.9$ , and  $r_- = r_+ = 0.25$ . The length of the generated sentence by the language model,  $N$ , was varied from 16 to 4096.

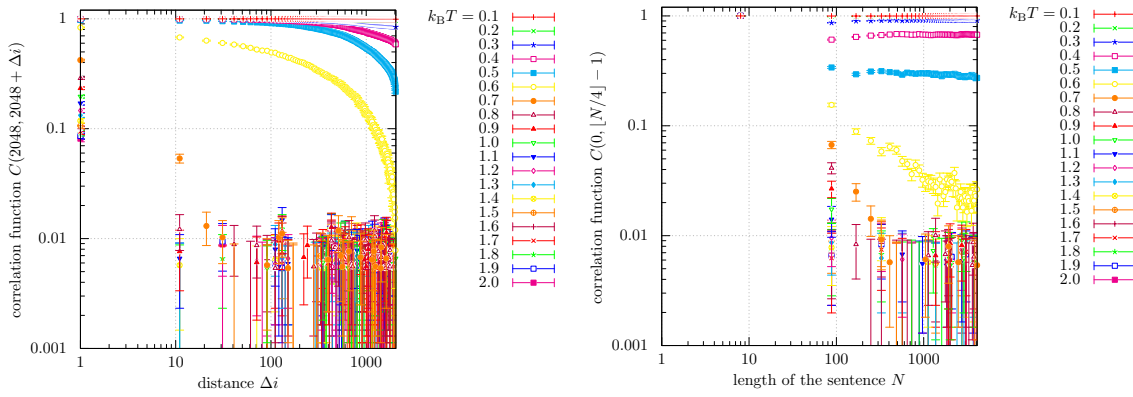


FIG. S-52: Correlation functions, Eq. (S-3.20) (left) with  $i = 2048$  and  $j = 2048 + \Delta i$  and (right) with  $i = 0$  and  $j = \lfloor N/4 \rfloor - 1$  for  $X \rightarrow XX$ . We set  $K = 10$ ,  $J = 1.0$ ,  $q = 10^{-2.0}$ ,  $t = 0$ ,  $s = 0.9$ , and  $r_- = r_+ = 0.25$ . Temperature  $k_B T$  was varied from 0.1 to 2.0.

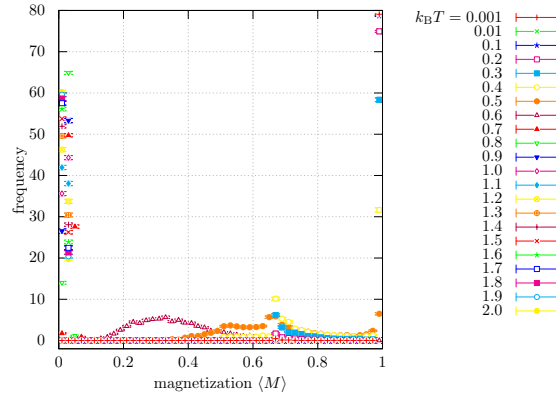


FIG. S-53: Histogram of the magnetization, Eq. (S-3.1), for  $X \rightarrow XX$ . We set  $K = 10$ ,  $J = 1.0$ ,  $q = 10^{-2.0}$ ,  $t = 0$ ,  $s = 0.9$ , and  $r_- = r_+ = 0.25$ . Temperature  $k_B T$  was varied from 0.1 to 2.0.

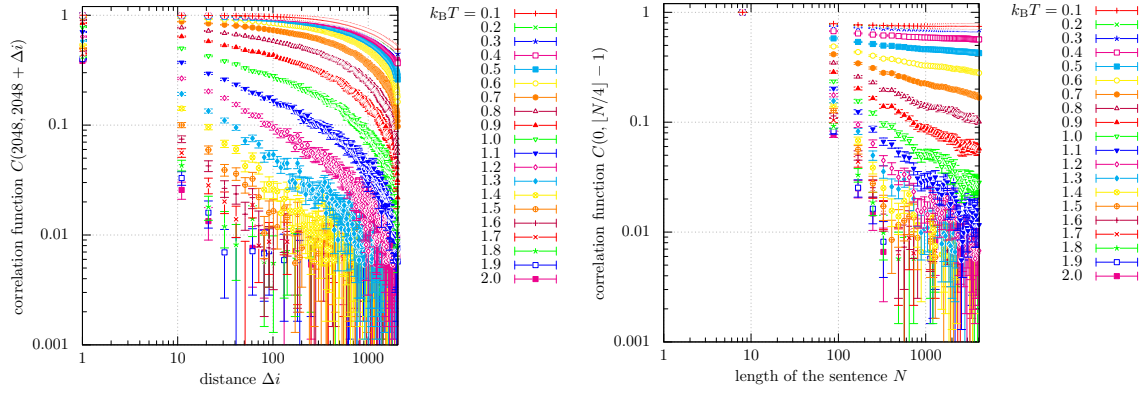


FIG. S-54: Correlation functions, Eq. (S-3.20) (left) with  $i = 2048$  and  $j = 2048 + \Delta i$  and (right) with  $i = 0$  and  $j = \lfloor N/4 \rfloor - 1$  for  $X \rightarrow XX$ . We set  $K = 10$ ,  $J = 1.0$ ,  $q = 10^{-0.5}$ ,  $t = 0$ ,  $s = 0.9$ , and  $r_- = r_+ = 0.25$ . Temperature  $k_B T$  was varied from 0.1 to 2.0.

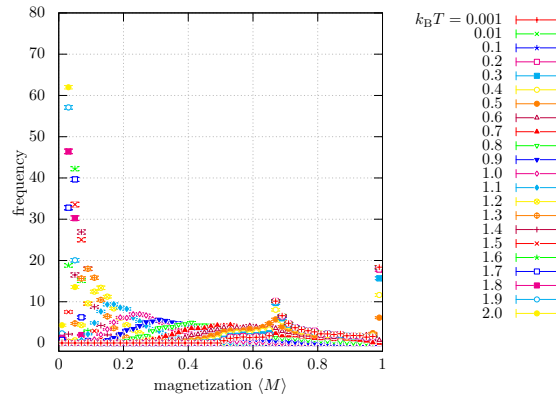


FIG. S-55: Histogram of the magnetization, Eq. (S-3.1), for  $X \rightarrow XX$ . We set  $K = 10$ ,  $J = 1.0$ ,  $q = 10^{-0.5}$ ,  $t = 0$ ,  $s = 0.9$ , and  $r_- = r_+ = 0.25$ . Temperature  $k_B T$  was varied from 0.1 to 2.0.

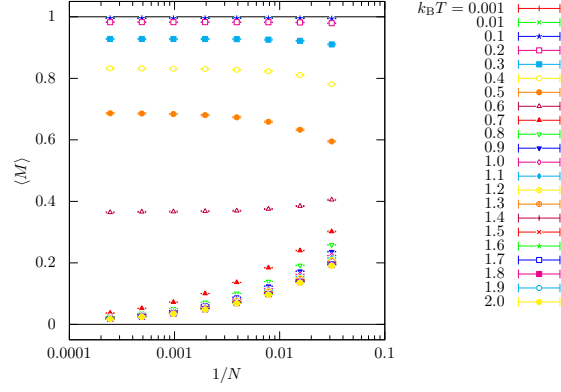


FIG. S-56: System-size dependence of the magnetization, Eq. (S-3.1), at  $q = 10^{-2.0}$ . We consider  $X \rightarrow XX$  and set  $K = 10$ ,  $J = 1.0$ ,  $t = 0$ ,  $s = 0.9$ , and  $r_- = r_+ = 0.25$ . We varied  $N = 32, 64, 128, 256, 512, 1024, 2048, 4096$ .

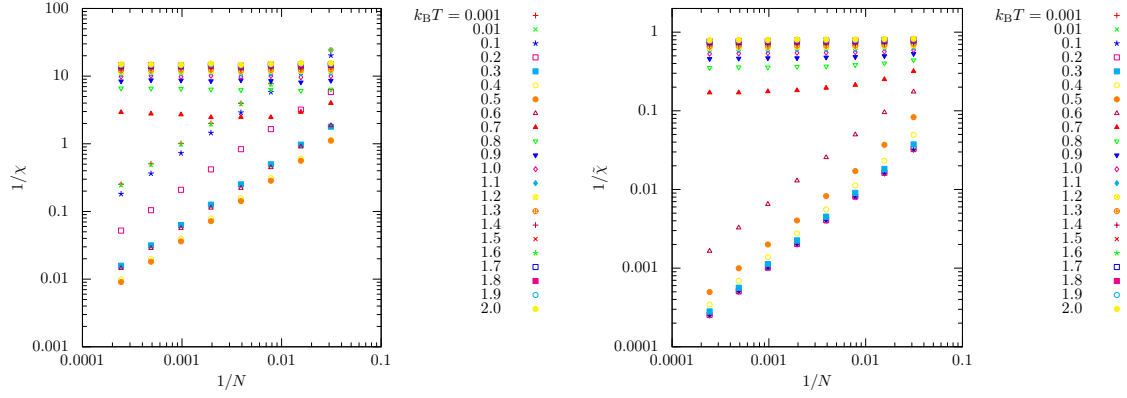


FIG. S-57: System-size dependence of the susceptibilities, (left) Eq. (S-3.12) and (right) Eq. (S-3.15) at  $q = 10^{-2.0}$ . We consider  $X \rightarrow XX$  and set  $K = 10$ ,  $J = 1.0$ ,  $t = 0$ ,  $s = 0.9$ , and  $r_- = r_+ = 0.25$ . We varied  $N = 32, 64, 128, 256, 512, 1024, 2048, 4096$ .

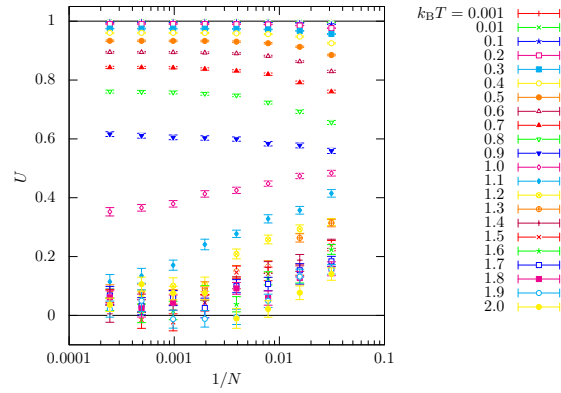


FIG. S-58: System-size dependence of the Binder parameter, Eq. (S-3.17), at  $q = 10^{-2.0}$ . We consider  $X \rightarrow XX$  and set  $K = 10$ ,  $J = 1.0$ ,  $t = 0$ ,  $s = 0.9$ , and  $r_- = r_+ = 0.25$ . We varied  $N = 32, 64, 128, 256, 512, 1024, 2048, 4096$ .

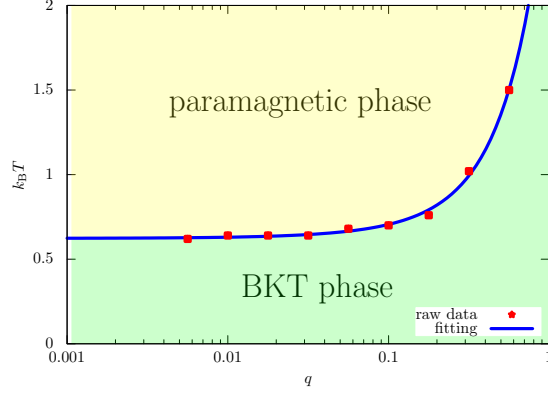


FIG. S-59: Phase diagram of the CSG model investigated in this paper where the horizontal and vertical axes are the growth rate of a sentence  $q$  and temperature  $k_B T$ , respectively. We consider  $X \rightarrow XX$  and set  $K = 10$ ,  $J = 1.0$ ,  $t = 0$ ,  $s = 0.9$ , and  $r_- = r_+ = 0.25$ .

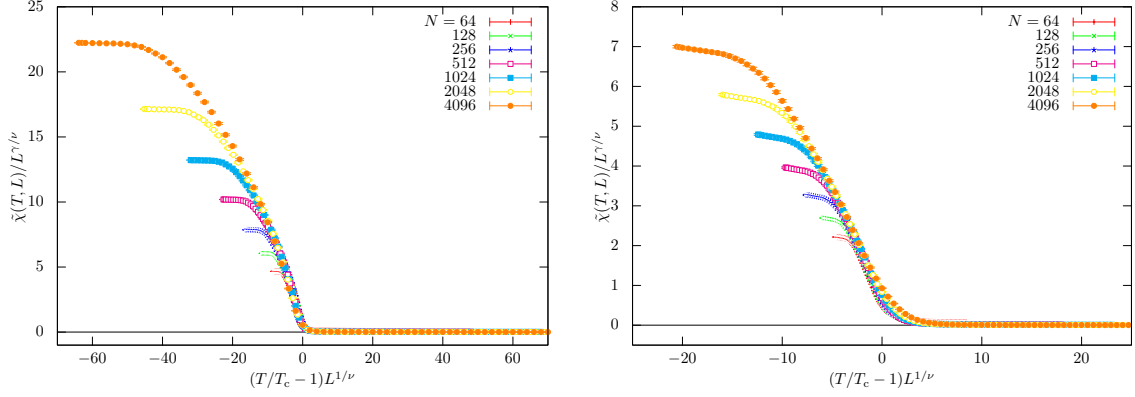


FIG. S-60: Finite-size scaling of  $\tilde{\chi}$  at (left)  $q = 10^{-2.0}$  and (right)  $q = 10^{-1.0}$ . We set  $T_c = 0.640$ ,  $\nu = 2.0$ , and  $\gamma = 1.25$  for  $q = 10^{-2.0}$  and  $T_c = 0.70$ ,  $\nu = 2.75$ , and  $\gamma = 2.05$  for  $q = 10^{-1.0}$ , where the values of  $\nu$  and  $\gamma$  are determined such that the scaling assumption is satisfied. We consider  $X \rightarrow XX$  and set  $K = 10$ ,  $J = 1.0$ ,  $t = 0$ ,  $s = 0.9$ , and  $r_- = r_+ = 0.25$ . We varied  $N = 64, 128, 256, 512, 1024, 2048, 4096$ .

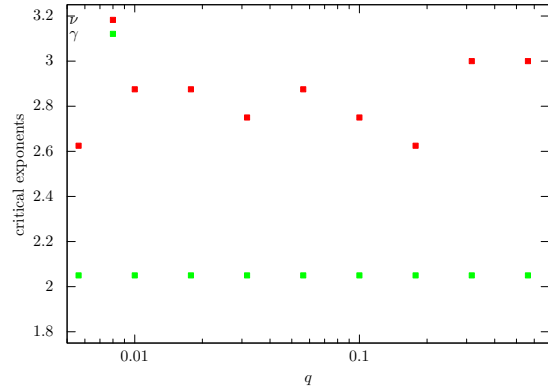


FIG. S-61:  $q$ -dependence of the critical exponents  $\nu$  and  $\gamma$ . We consider  $X \rightarrow XX$  and set  $K = 10$ ,  $J = 1.0$ ,  $t = 0$ ,  $s = 0.9$ , and  $r_- = r_+ = 0.25$ .

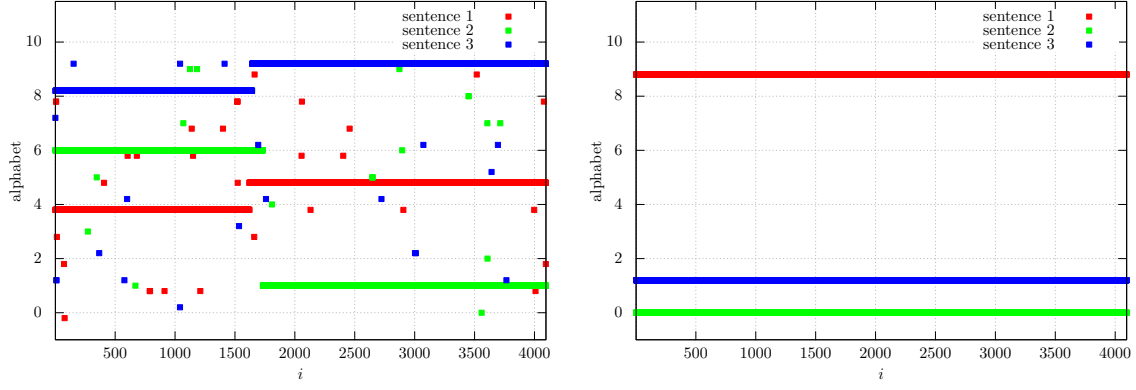


FIG. S-62: Typical configurations of symbols for  $X \rightarrow XX$ . (left) We considered states of which magnetization lies between 0.6600 and 0.6800 at  $k_B T = 0.440$ , and (right) state of which magnetization lies between 0.9800 and 1.0000 at  $k_B T = 0.0010$ . We set  $K = 10$ ,  $J = 1.0$ ,  $q = 10^{-2.0}$ ,  $t = 0$ ,  $s = 0.9$ , and  $r_- = r_+ = 0.25$ .

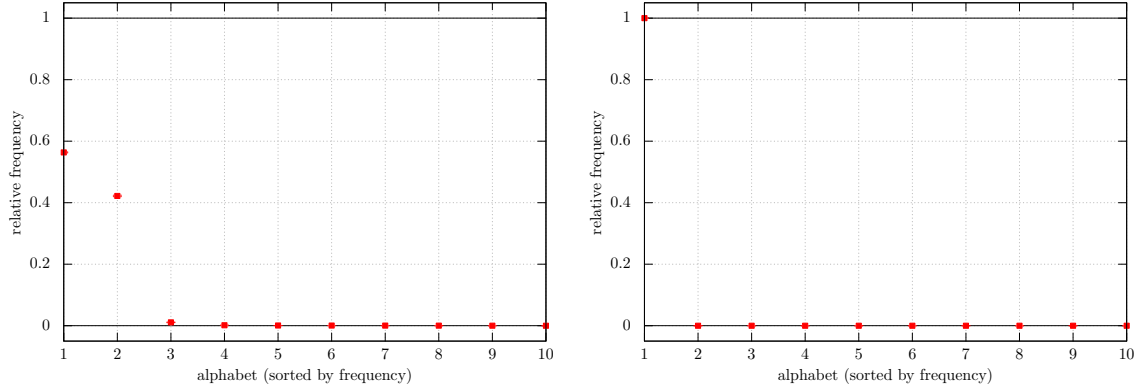


FIG. S-63: Relative frequencies of alphabets for  $X \rightarrow XX$ . (left) We considered states of which magnetization lies between 0.6600 and 0.6800 at  $k_B T = 0.440$ , and (right) state of which magnetization lies between 0.9800 and 1.0000 at  $k_B T = 0.0010$ . We set  $K = 10$ ,  $J = 1.0$ ,  $q = 10^{-2.0}$ ,  $t = 0$ ,  $s = 0.9$ , and  $r_- = r_+ = 0.25$ . Symbols on the horizontal axis are sorted by frequencies. The scales of the vertical and horizontal axes are linear.

- 
- [1] M. Sipser, *Introduction to the Theory of Computation* (Cengage Learning, 2012), ISBN 9781133187790, URL <https://books.google.co.jp/books?id=H94JzgEACAAJ>.
  - [2] E. DeGiuli, *Phys. Rev. Lett.* **122**, 128301 (2019), URL <https://link.aps.org/doi/10.1103/PhysRevLett.122.128301>.
  - [3] E. D. Giuli, *Journal of Physics A: Mathematical and Theoretical* **52**, 504001 (2019), URL <https://doi.org/10.1088/1751-8121/ab293c>.
  - [4] K. Nakaishi and K. Hukushima, *Phys. Rev. Research* **4**, 023156 (2022), URL <https://link.aps.org/doi/10.1103/PhysRevResearch.4.023156>.
  - [5] F. Lalegani and E. De Giuli, arXiv preprint arXiv:2309.14913 (2023).
  - [6] S. Stengele, D. Drexel, and G. De las Cuevas, *Proceedings of the Royal Society A: Mathematical, Physical and Engineering Sciences* **479**, 20220553 (2023), <https://royalsocietypublishing.org/doi/pdf/10.1098/rspa.2022.0553>, URL <https://royalsocietypublishing.org/doi/abs/10.1098/rspa.2022.0553>.
  - [7] F. J. Dyson, *Matematika* **16**, 137 (1972).
  - [8] J. Fröhlich and T. Spencer (1982).
  - [9] F. J. Dyson, *Matematika* **16**, 113 (1972).
  - [10] F. J. Dyson, *Communications in Mathematical Physics* **21**, 269 (1971).
  - [11] D. J. Thouless, *Phys. Rev.* **187**, 732 (1969), URL <https://link.aps.org/doi/10.1103/PhysRev.187.732>.
  - [12] Y. Chang, L. Sun, and X. Cai, *Phys. Rev. E* **76**, 021101 (2007), URL <https://link.aps.org/doi/10.1103/PhysRevE.76.021101>.
  - [13] J. Martínez-Herrera, O. Rodríguez-López, and M. Solís, *Physica A: Statistical Mechanics and its Applications* **596**, 127136 (2022), ISSN 0378-4371, URL <https://www.sciencedirect.com/science/article/pii/S0378437122001534>.
  - [14] Y. Tomita, *Journal of the Physical Society of Japan* **78**, 014002 (2009), <https://doi.org/10.1143/JPSJ.78.014002>, URL <https://doi.org/10.1143/JPSJ.78.014002>.
  - [15] Y. Chang, L. Sun, and X. Cai, *Phys. Rev. E* **76**, 021101 (2007), URL <https://link.aps.org/doi/10.1103/PhysRevE.76.021101>.
  - [16] F. Y. Wu, *Rev. Mod. Phys.* **54**, 235 (1982), URL <https://link.aps.org/doi/10.1103/RevModPhys.54.235>.
  - [17] J. M. Kosterlitz, *Phys. Rev. Lett.* **37**, 1577 (1976), URL <https://link.aps.org/doi/10.1103/PhysRevLett.37.1577>.
  - [18] J. M. Kosterlitz, *Reports on Progress in Physics* **79**, 026001 (2016), URL <https://dx.doi.org/10.1088/0034-4885/79/2/026001>.
  - [19] E. Luijten, *Interaction range, universality and the upper critical dimension* (1997).
  - [20] M. Krech and E. Luijten, *Phys. Rev. E* **61**, 2058 (2000), URL <https://link.aps.org/doi/10.1103/PhysRevE.61.2058>.
  - [21] M. Aizenman and R. Fernández, *Letters in Mathematical Physics* **16**, 39 (1988).
  - [22] M. Aizenman, J. T. Chayes, L. Chayes, and C. M. Newman, *Journal of Statistical Physics* **50**, 1 (1988).
  - [23] K. Fukui and S. Todo, *Journal of Computational Physics* **228**, 2629 (2009).
  - [24] Y. Kumano, K. Hukushima, Y. Tomita, and M. Oshikawa, *Phys. Rev. B* **88**, 104427 (2013), URL <https://link.aps.org/doi/10.1103/PhysRevB.88.104427>.
  - [25] Y. Miyajima, Y. Murata, Y. Tanaka, and M. Mochizuki, *Phys. Rev. B* **104**, 075114 (2021), URL <https://link.aps.org/doi/10.1103/PhysRevB.104.075114>.
  - [26] A. W. Sandvik, in *AIP Conference Proceedings* (American Institute of Physics, 2010), vol. 1297, pp. 135–338.
  - [27] D. Landau and K. Binder, *A Guide to Monte Carlo Simulations in Statistical Physics* (Cambridge University Press, 2021), ISBN 9781108490146, URL <https://books.google.co.jp/books?id=WW8yEAAAQBAJ>.
  - [28] M. Fujimoto and H. Otsuka, *Phys. Rev. E* **102**, 032141 (2020), URL <https://link.aps.org/doi/10.1103/PhysRevE.102.032141>.
  - [29] H. W. Lin and M. Tegmark, *Entropy* **19** (2017), ISSN 1099-4300, URL <https://www.mdpi.com/1099-4300/19/7/299>.
  - [30] K. Nakaishi and K. Hukushima, arXiv preprint arXiv:2402.07113 (2024).